水に富む系外惑星の熱進化と質量散逸

○黒崎健二 (1,2)　生駒大洋 (2)　堀安範 (3)
(1) 東京工業大学　(2) 東京大学　(3) 国立天文台

2012 年 8 月 2 日発表

Abstract

近年の観測技術の発達により、検出された系外惑星の数は 700 を超えた。地球質量の 30 倍以下という比較的小質量の惑星（以降「スーパーアース」と表記する）の発見数も増加しており、31 個のスーパーアースについては質量に加えて半径も推定されている（2012 年 8 月 23 日現在、www.exoplanet.eu より）。それらのスーパーアースの中には、水に富むと考えられるスーパーアース（例えば GJ1214b）もある（e.g. Rogers & Seager 2010; Nettelmann et al. 2011）。発見された系外惑星を質量―半径関係図上に表してみると、温度の効果を考慮しない状態方程式を用いて求めた理論的な質量―半径関係（e.g. Seager et al. 2007）と比べて、質量とともに半径が増加するという傾向は同じだが、発見された系外惑星の方がその増加率が大きいことに気づく。一方、これまでに発見されたスーパーアースは中心星近傍に存在しているため、強烈な X 線や UV（XUV）の照射に晒され、質量散逸（大気散逸）を経験してきたはずである。しかし、その効果に対する質量―半径関係図上での系統的な議論はこれまでにされていない。今後、多数発見されると期待されるスーパーアースの質量と半径の傾向を理解することは、惑星の組成や起源を考察する上で重要である。本研究では水に富むスーパーアースに注目し、岩石コアを水のマントルが覆う惑星の熱進化計算を行った。そして、(i) 中心星放射による加熱の効果を考慮した惑星の質量―半径関係と、(ii) 質量散逸を考慮した場合の質量―半径関係をそれぞれ求めた。その結果、(i) 中心星放射による加熱の効果を考慮した理論的な質量―半径関係と発見された系外惑星のそれを比較すると、軽い惑星ほど水成分が少ない傾向にあることがわかった。また、(ii) 質量散逸を考慮した場合、初期に低質量で半径が大きかった惑星は、水成分が散逸して質量が小さくなりやすいことがわかった。このことから、惑星の水成分が散逸することで岩石成分の割合が大きくなり、水成分の層が薄くなって惑星半径が小さくなることもわかった。これらの結果は、惑星の質量―半径関係図上で水に富むスーパーアースが存在しうる領域に制限をあたえることができる.

1 Introduction

Recent progress in the observation enabled us to find over 700 exoplanets, including low-mass exoplanets whose masses are less than $30M_{\oplus}$. According to exoplanets' database (www.exoplanet.eu), we can know 31 low-mass planets' masses and radii. Given the planet's mass and radius, we find the planet's mean density. The planet's mean density has a clue to understand the planet's composition and origin.

Increasing the number of exoplanets gives us the useful statistical information. To analyze the statistical information, we show the exoplanets on the mass-radius relationship. Comparing with the mass-radius relation ship of the solid planets (e.g. Seager et al. 2007, Fortney et al. 2007), we fan find as the planet's mass increase its radius also increase while the radius increasing rate of exoplanets is steeper than that of solid planets. To explain the difference, we need to consider the planet's expansion due to the thermal effect. Short-period exoplanets must have experienced the mass loss because of the intense stellar X-ray and UV (XUV) flux. However, effect of the mass loss on the mass-radius relationship have not discussed yet. It is important to understand the mass-radius relationship of the low-mass planet for discussing the planet's composition and origin.

In this study, we calculate the thermal evolution and mass loss of the water-rich planet which is consisted of the rocky core and the water mantle. And we derive (i) the mass-radius relationship of the water-rich planet taking into account the effect of irradiation of the host star and (ii) the mass-radius relationship taking into account the mass loss of the planet.

2 Method

We assume the planet is spherically-symmetric three layer structure which is consisted of isothermal rocky core, convective water layer and radiative water vapor atmosphere form inside out. We deal with the thermal evolution and the mass loss driven by stellar XUV flux simultaneously.

2.1 Atmospheric model

We assume the planet's atmosphere has plain-parallel radiative equilibrium structure. We make use of radiative momentum equations derived by Guillot (2010);

$$\frac{dH_{\rm v}}{dm} = \kappa_{\rm v}^{p} J_{\rm v}, \tag{1}$$

$$\frac{dK_{\rm v}}{dm} = \kappa_{\rm v}^{r} H_{\rm v}, \tag{2}$$

$$\frac{dH_{\rm th}}{dm} = \kappa_{\rm th}^{p} \left(J_{\rm th} - B \right), \tag{3}$$

$$\frac{dK_{\rm th}}{dm} = \kappa_{\rm th}^{r} H_{\rm th}, \tag{4}$$

$$\kappa_{\rm v}^{p} J_{\rm v} + \kappa_{\rm th}^{p} \left(J_{\rm th} - B \right) = 0, \tag{5}$$

where H, J, K are the moment of radiative transfer equation whose subscript means wavelength (v: visible, th: thermal), m is atmospheric mass coordinate, B is the Planck function, and κ is the mean opacity;

$$\kappa_{\rm v}^{p} := \int_{\rm v} \kappa_\nu J_\nu d\nu \Big/ \int J_\nu d\nu, \tag{6}$$

$$\frac{1}{\kappa_{\rm v}^{r}} := \int_{\rm v} \frac{1}{\kappa_\nu} \frac{{\rm d}H_\nu}{{\rm d}m} d\nu \Big/ \int \frac{dH_\nu}{dm} d\nu, \tag{7}$$

$$\kappa_{\rm th}^{p} := \int_{\rm th} \kappa_\nu J_\nu d\nu \Big/ \int J_\nu d\nu, \tag{8}$$

$$\frac{1}{\kappa_{\rm th}^{r}} := \int_{\rm th} \frac{1}{\kappa_\nu} \frac{{\rm d}H_\nu}{{\rm d}m} d\nu \Big/ \int \frac{dH_\nu}{dm} d\nu, \tag{9}$$

respectively (subscript "v" means visible light frequency, "th" means thermal or infrared light frequency). Practically in this paper, we deal with these opacities as

the Planck mean opacities or the Rosseland mean opacities;

$$\kappa_{\rm v}^{p} = \int \kappa_\nu B_\nu(T=T_\star)d\nu \Big/ \int B_\nu(T=T_\star)d\nu, \tag{10}$$

$$\frac{1}{\kappa_{\rm v}^{r}} = \int \frac{1}{\kappa_\nu}\frac{{\rm d}B_\nu(T=T_\star)}{{\rm d}T}d\nu \Big/ \int \frac{dB_\nu(T=T_\star)}{dT}d\nu, \tag{11}$$

$$\kappa_{\rm th}^{p} = \int \kappa_\nu B_\nu(T=T_{\rm atm})d\nu \Big/ \int B_\nu(T=T_{\rm atm})d\nu, \tag{12}$$

$$\frac{1}{\kappa_{\rm th}^{r}} = \int \frac{1}{\kappa_\nu}\frac{{\rm d}B_\nu(T=T_{\rm atm})}{{\rm d}T}d\nu \Big/ \int \frac{dB_\nu(T=T_{\rm atm})}{dT}d\nu, \tag{13}$$

where $B_\nu(T)$ is the Planck function, $T_\star$ is the temperature of host star, and $T_{\rm atm}$ is the temperature of the atmosphere respectively. We adopt HITRAN opacity data fitted by the least square method;

$$\kappa_{\rm v}^{p} = 697\left(\frac{P}{1{\rm bar}}\right)^{2.07E-2} \tag{14}$$

$$\kappa_{\rm v}^{r} = 0.0137\left(\frac{P}{1{\rm bar}}\right)^{0.983} \tag{15}$$

$$\kappa_{\rm th}^{p} = 365\left(\frac{P}{1{\rm bar}}\right)^{8.88E-3}\left(\frac{T}{1000{\rm K}}\right)^{-2.06}, \tag{16}$$

$$\kappa_{\rm th}^{r} = 0.240\left(\frac{P}{1{\rm bar}}\right)^{0.929}\left(\frac{T}{1000{\rm K}}\right)^{-2.03}, \tag{17}$$

where P is pressure, T is temperature respectively. We fit HITRAN opacity data table at $P = 1, 10, 100, 1000$ and $T = 1000, 2000, 3000$K

We assume Eddington approximation;

$$K_{\rm v} = \frac{1}{3}J_{\rm v}, \tag{18}$$

$$K_{\rm th} = \frac{1}{3}J_{\rm th}. \tag{19}$$

The boundary condition of the moment equation is

$$H = H_{\rm v} + H_{\rm th} = \frac{1}{4\pi}\sigma T_{\rm int}^4, \tag{20}$$

$$H_{\rm v}(m=0) = -\frac{1}{\sqrt{3}}\frac{1}{4\pi}\sigma T_{\rm irr}^4, \tag{21}$$

where $T_{\rm int}$ is intrinsic temperature, $T_{\rm irr}$ is irradiation temperature, respectively. And upper boundary condition between J and H, we use

$$H_{\rm v}(m=0) = -\frac{1}{\sqrt{3}} J_{\rm v}(m=0), \tag{22}$$

$$H_{\rm th}(m=0) = \frac{1}{2} J_{\rm th}(m=0). \tag{23}$$

We treat the bottom of atmosphere as the interface between radiative and convective zone. We use Schwarzschild criterion to determine the interface. If the temperature gradient $\nabla := d\ln T/d\ln P$ is lager than adiabatic temperature gradient $\nabla_{\rm ad}$, i.e. $\nabla > \nabla_{\rm ad}$, the heat transport system by the convection become dominate rather than by the radiation. We use ($P_{\rm ad}$, $T_{\rm ad}$) as the boundary condition of the interior structure of the planet.

We calculate the pressure and optical depth by hydrostatic equilibrium;

$$\frac{\partial P}{\partial m} = g, \tag{24}$$

$$\frac{\partial \tau}{\partial m} = \kappa^r_{\rm th}. \tag{25}$$

We assume the atmosphere is plain-parallel approximation. The optical depth is evaluated by $\kappa^r_{\rm th}$, and the planetary radius is determined at $\tau = 2/3$. The atmospheric thickness z is evaluated by

$$z = \int_{2/3}^{\tau_{ad}} \frac{H}{\tau} d\tau = \frac{\mathcal{R}}{\mu g} \int_{2/3}^{\tau_{ad}} \frac{T}{\tau} d\tau, \tag{26}$$

where H is scale hight $H := dr/d\ln P$, $\mathcal{R}$ is gas constant, μ is molecular weight and τ_{ad} is the optical depth at the interface between radiative layer and convective layer. We assume that atmosphere's gas is behaved as an ideal gas.

2.2 Interior structure

The boundary condition is determined by the atmospheric model; $(P_{\rm ad}, T_{\rm ad})$, determined by the Schwarzschild criterion; $\nabla = \nabla_{\rm ad}$. We assume the interior structure of the planet is spherically-symmetric, hydrostatic equilibrium;

$$\frac{\partial P}{\partial M_r} = -\frac{GM_r}{4\pi r^4}, \tag{27}$$

$$\frac{\partial r}{\partial M_r} = \frac{1}{4\pi r^2}, \tag{28}$$

where M_r is interior mass coordinate, r is the distance from the planet center, P is the pressure, ρ is the density and G is the gravitational constant respectively.

In the water layer, we also assume the temperature structure of the planet's interior follows adiabatic temperature; $T = T(P, S)$, where T is the temperature, P is the pressure and S is the entropy respectively. The equation of state we adopt is SESAME water EOS table whose serial number is 7150-301.

In the rock core, we have an assumption that rocky core is isothermal. We adopt the equation of state of rock is

$$P = \rho^{4.406} \exp\left(-6.579 - 0.176\rho + 0.00202\rho^2\right), \tag{29}$$

where ρ is in g/cm^3 and P is in Mbar, composed of 38% SiO_2, 25% MgO, 25% FeS, and 12% FeO. (Hubbard & Marley (1989))

We integrate straightforward from outer boundary $(P_{\rm ad}, T_{\rm ad})$ and iterate until the inner boundary is consistent with $r = 0, m = 0$.

We neglect the presence of any radioactive heat source in the interior. Therefore, the thermal evolution is determined by the equation of energy conservation;

$$\frac{\partial L}{\partial M_r} = -T\left(\frac{\partial \bar{S}}{\partial t}\right), \tag{30}$$

where L is the intrinsic luminosity, $\bar{S}$ is the entropy per unit mass (specific entropy), and t is time. To derive the simplified formula, we integrating this equation by mass,

$$-L_p = \left(\frac{\partial \bar{S}}{\partial t}\right)\int_{M_c}^{M_p} T dm + C_{\rm v} M_c \frac{\partial T_c}{\partial t}. \tag{31}$$

Note that the specific entropy is constant through the convective region and the core is isothermal. L_p is total intrinsic luminosity of the planet, $C_{\rm v}$ is the heat capacity of the rocky core, M_c is the mass of the core and T_c is the temperature of the rocky core respectivery. The formula of L_p is

$$L_p := \int_0^{M_p} \frac{\partial L}{\partial M_r} dM_r = 4\pi R_p^2 \sigma T_{\rm int}^4, \tag{32}$$

where M_p is the total mass of the planet, R_p is the planet radius, and $T_{\rm int}$ is the intrinsic temperature. We assume $C_{\rm v} = 10^7$ ergs/(K·g).

2.3 Mass loss

Erkaev et al. (2007) derived energy-limited XUV driven hydrodynamic escape;

$$\dot{M} = -\frac{\epsilon F_{\rm XUV} R_p \pi R_{\rm exo}^2}{G M_p K_{\rm tide}}, \tag{33}$$

where $\dot{M}$ is the mass loss rate per second, ϵ is the mass loss efficiency, $F_{\rm XUV}$ is X-ray and UV flux of the host star, R_p is the radius of the planet, $R_{\rm exo}$ is the exobase of the planet, M_p is the mass of the planet, $K_{\rm tide}$ is Roche-lobe effect, and G is gravitation constant. We suppose that the host star is G-star and $F_{\rm XUV}$ is

$$F_{\rm XUV} = 29.7 \left(\frac{t}{1{\rm Gyr}}\right)^{-1.23} \left(\frac{a}{1{\rm AU}}\right)^{-2} {\rm erg}/({\rm s}\cdot{\rm cm}^2), \tag{34}$$

derived by Ribas et al. (2005) when the host star's age t is $0.1{\rm Gyr} \leq t \leq 6.7{\rm Gyr}$. The XUV flux before 0.1 Gyr is uncertain. We assume the XUV flux is constant before 0.1 Gyr;

$$F_{\rm XUV} = 504 \left(\frac{a}{1{\rm AU}}\right)^{-2} {\rm erg}/({\rm s}\cdot{\rm cm}^2), \tag{35}$$

and we also assume that the XUV flux is decline following the power law; $t^{-1.23}$. The formula of $K_{\rm tide}$ is derived by Erkaev et al. (2007);

$$K_{\rm tide} = \frac{(\eta-1)^2(2\eta+1)}{2\eta^3}, \tag{36}$$

where $\delta = M_p/M_\odot$, $\lambda = a/R_p$, $\eta = r_{\rm RL}/R_p$ ($r_{\rm RL}$ means Roche-lobe radius; $r_{\rm RL} \approx (\delta/3)^{1/3}d$) respectively. $R_{\rm exo}$ and ϵ are related to the atmospheric composition and the chemical reaction. We assume $R_{\rm exo} = R_p$ and $\epsilon = 0.1$. We calculate quasi-static thermal evolution and mass loss.

2.4 The procedure to calculate the interior structure and evolution of the planet.

The planet's radius R_p is determined by the planet's mass M_p, the planet's specific entropy $\bar{S}$ and the water to rock ratio $X_{w/r}$. The planet's radius R_p is described by the sum of the planet's convective zone radius $R_{\rm conv}$ and the thickness of the atmosphere z. That is, $R_p = R_{\rm conv} + z$. We integrate the hydrostatic equations by 4th-order Runge-Kutta method and use shooting method to determine the planet's convective zone radius $R_{\rm conv}$. The planet's specific entropy $\bar{S}$ is the important parameter to determine the planet's thermal evolution. To calculate $\bar{S}$, we integrate the radiative momentum equations of the planet's atmosphere.

To calculate the thermal evolution of the planet, we derive the evolution time Δt which correspond to $\Delta\bar{S}$. We also calculate the mass loss $M(t+\Delta t) - M(t) = \dot{M}\Delta t$.

Our interior structure code is checked by Valencia et al. (2007) and the atmospheric code is checked by the analytical formula derived by Guillot(2010).

3 Result

3.1 The atmospheric structure

Figure 1 shows the planet's atmospheric structure. We calculate the planet's atmospheric structure composed of water provided that the planet's mass is $10M_{\oplus}$, its semi-major axis is 0.05AU and water to rock ratio is 3. We parametrized the planet's luminosity $L_{p,0} = 10^{23}, 10^{24}, 10^{25}, 10^{26}$ ergs/s. The bottom of the atmosphere is determined by Schwarzschild criterion; $\nabla = \nabla_{\rm ad}$. We find as the planet lose its heat, the pressure at the interface between radiative layer and convective layer, $P_{\rm ad}$, becomes large. This trend corresponds to losing planet's entropy by the thermal evolution of the planet.

3.2 Planetary evolution without mass loss

We show results which the water-rich planet experiences shrinkage due to the cooling.

Figure 2 shows the mass-radius relationship of the water-rich planets. We derive isochron lines of 10 giga years. We assume the water to rock ratio $X_{w/r}$ =0.1, 0.3, 1, 3 and 10. These relationships shows following two features:

- Planets' radii have weak dependence on their mass at $X_{w/r} \geq 1$.
- As masses of planets whose $X_{w/r} = 0.1$ become large, their radii also become large. However, they have gentler slop than the rocky planet's slope on the mass-radius relationship.

Here, we compare with the mass-radius relationship and the observed exoplanets. We can find that the slope of observations is steeper than that of the water-rich planets. This suggests that as planets become massive, planets seem to have more volatile compositions.

3.3 Planetary evolution with mass loss

In this subsection, we discuss the water-rich planets' evolution taking into account the energy limited hydrodynamic escape. Figure 3 shows the time evolution of planets' masses (upper) or radii (downer) including thermal evolution and mass loss simultaneously. We set the parameters that the initial luminosity of the planet is 10^{25} erg/s, the semi-major axis is $a = 0.05$AU, the water to rock ratio $X_{w/r} = 3$ and the mass loss efficiency $\epsilon = 0.1$. We show 4 examples: planets masses are $14, 15, 20$ and $30M_{\oplus}$. In this case, planets $M_p > 14M_{\oplus}$ remain their water layers and $M_p < 14M_{\oplus}$ lose their water layers at all. $14, 15$ and $20M_{\oplus}$ planets have typical time scales when their mass lose steeply. These time scales are $< 10^7$ years for $14M_{\oplus}$ planet, $\sim 10^7$ years

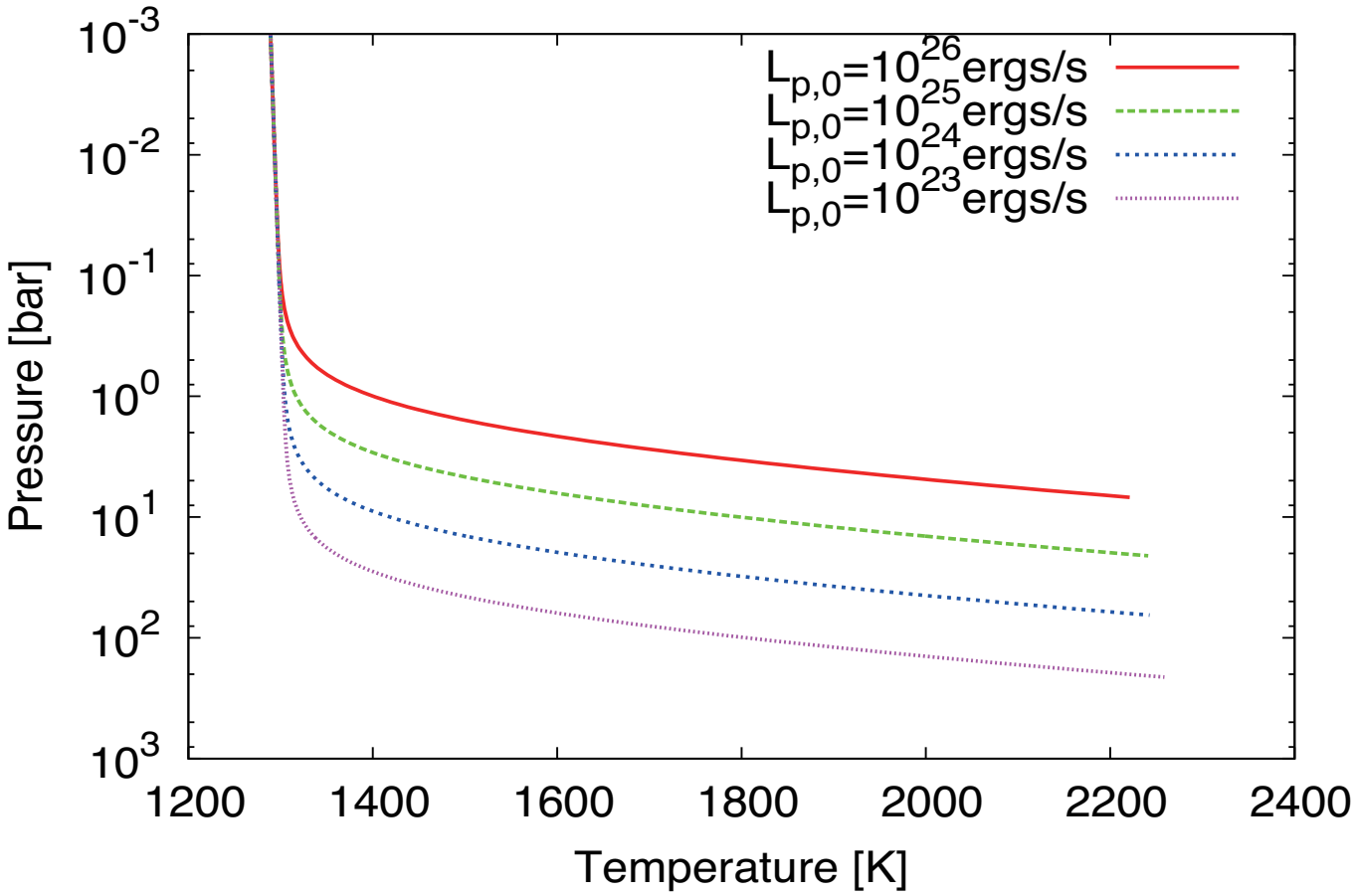

Figure 1: This figure shows atmospheric profile. The x-axis is the temperature [K] and the y-axis is the pressure [bar]. We set parameters $M_p = 10M_\oplus, a = 0.05$AU, and the water to rock ratio $X_{w/r} = 3$. We set the planet's luminosity $L_{p,0} = 10^{23}$(pink), 10^{24}(blue), 10^{25}(green) and 10^{26}(red). We calculate until the Schwarzschild criterion; $\nabla = \nabla_{\rm ad}$.

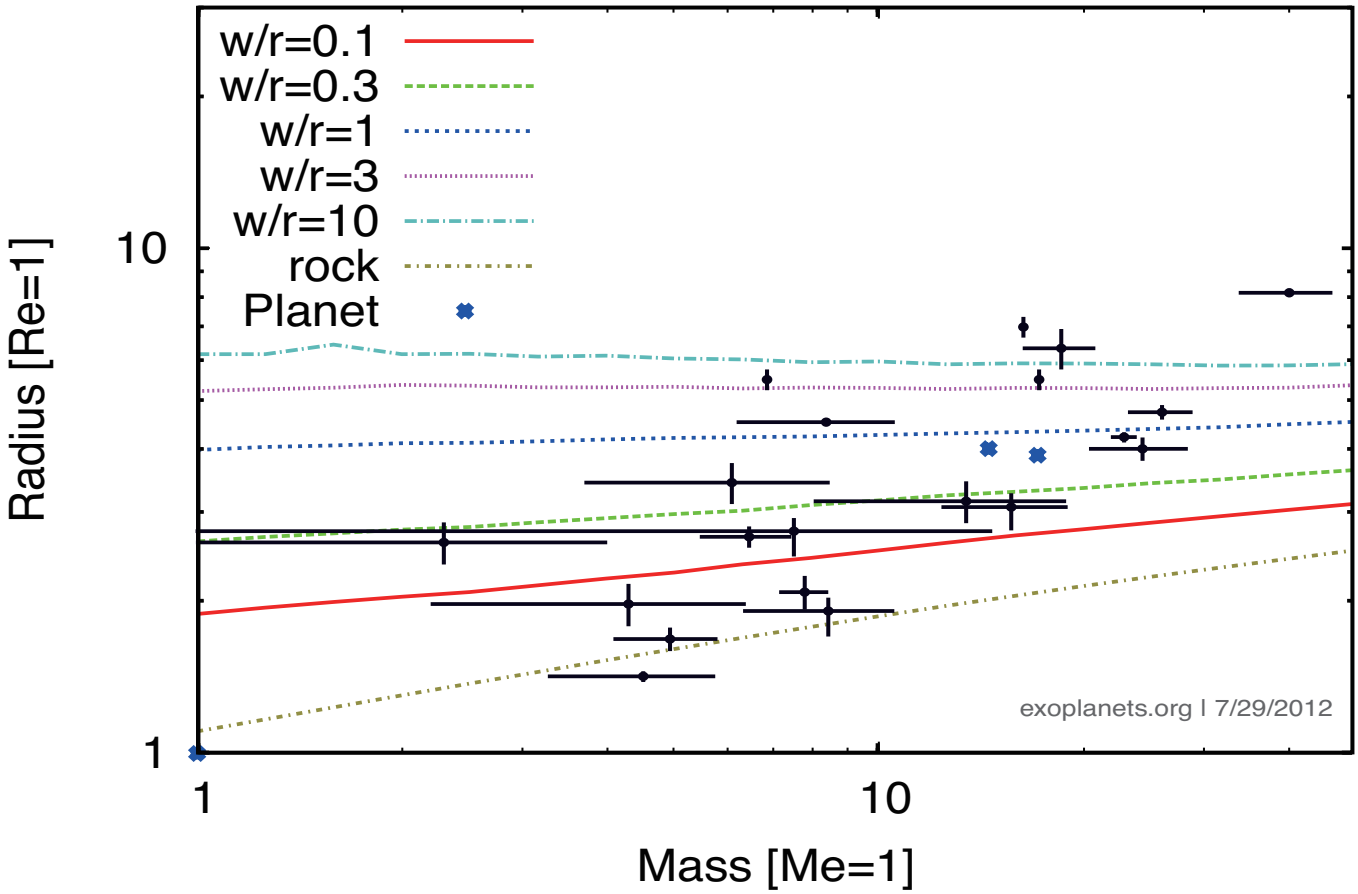

Figure 2: This figure shows the mass-radius relationship of water-rich planets. The x-axis is planets' mass $[M_\oplus]$ and the y-axis is planets' radii $[R_\oplus]$. We set parameters $a = 0.05$AU, water/rock $= 0.1, 0.3, 1, 3$ and 10. These isochron lines represent 10 giga years.

for $15M_\oplus$ planet and $\sim 10^8$ years for $20M_\oplus$ planet. At these time scales, planets' radii also slightly expand due to weaken the effect of the gravitational compression comparing with the effect of the thermal expansion. Because of $\dot{M} \propto R_p^3/M_p$, $\dot{M}$ decreases by order of magnitude after experienced the steep mass loss. After the steep mass loss, the planet's water to rock ratio $X_{w/r} \sim 0.1$. Therefore the planet's radius gradually shrink due to the effect of the rocky core. These results suggest that the effect of mass loss has significant effect on the planetary composition for the low mass planet, especially $\sim 10M_\oplus$. The planet's radius shrinks because the rock component become dominant. That is, the planetary radius varies due to not only thermal evolution but also mass loss.

Figure 4 shows the planets' evolutionary tracks on the mass-radius relationship. We set the initial planet's luminosity 10^{25} ergs/s, the semi-major axis is 0.05AU, the mass loss efficiency is 0.1 and the water to rock ratio is 3. We can find the radius of $14M_\oplus$ planet is nearly Roche lobe radius. If the planet's radius larger than its Roche lobe radius, the planet can be collapsed by the tidal force of the host star. The mass loss model we adopt cannot apply if the planet's radius is larger than its Roche lobe radius. If the planet's radius is larger than its Roche lobe radius, the planet's water layer will be quickly evaporated and turned to be the necked rocky core planet. In this paper we deal with the case the planet's radius is larger than its Roche lobe radius as the planet is removed its water layer.

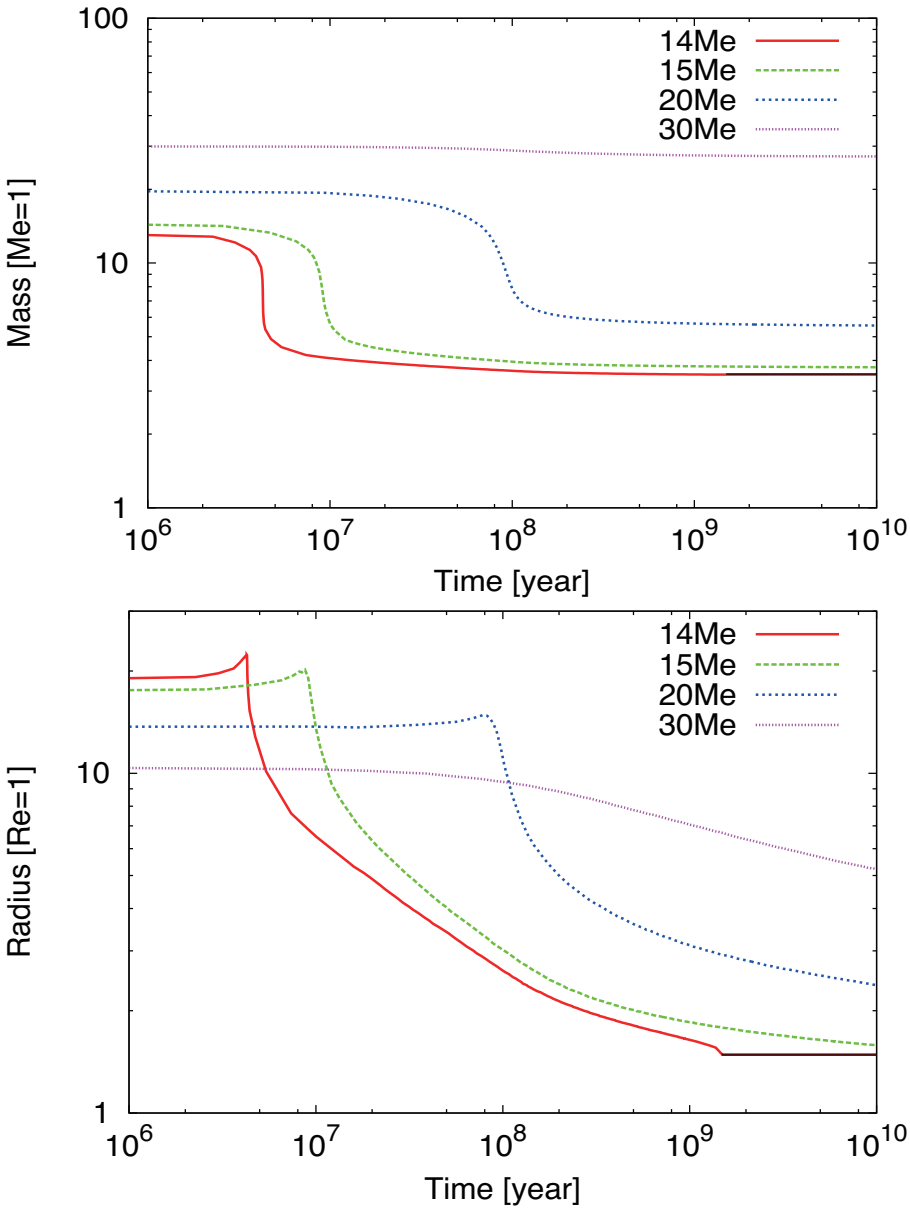

Figure 3: These figure shows time evolution of the planets' masses. (Upper) The x-axis is time [year] and the y-axis is planets' masses $[M_\oplus]$. (Downer) The x-axis is time [year] and the y-axis is planets' masses $[M_\oplus]$. We set parameters $L_{p,0} = 10^{25}$ergs/s, $a = 0.05$AU, $X_{w/r} = 3$ and $\epsilon = 0.1$. The red lines mean the planets whose planets' water mantle will evaporate at all and the brown lines connecting to red lines means necked rocky core. The blue lines means the planets which remain water layers for 10 giga years.

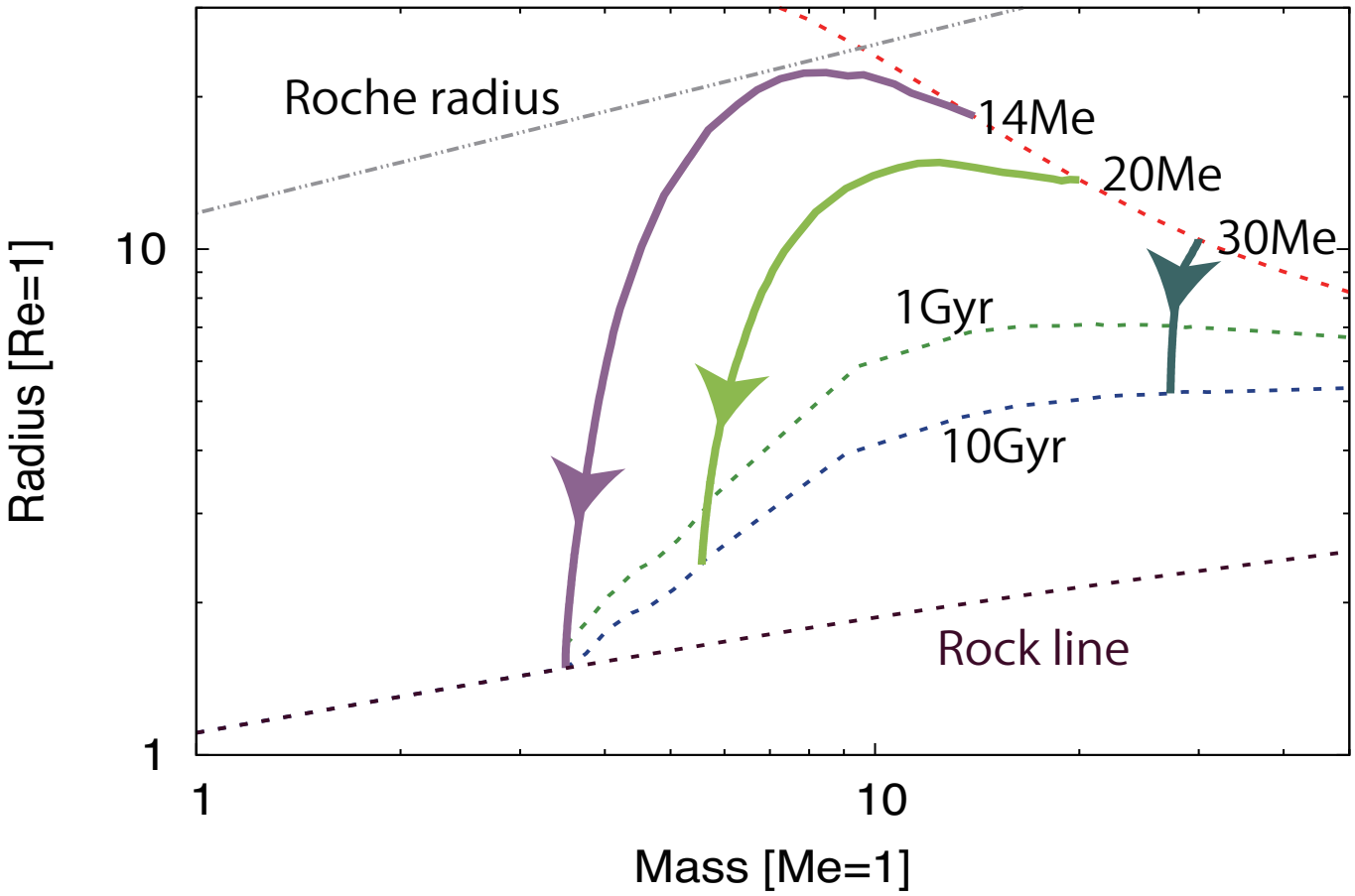

Figure 4: This figure shows the mass-radius relationship of the planets. The x-axis is planets' masses [$M_\oplus$], and the y-axis is planets' radii [$R_\oplus$]. The dotted lines mean the initial state of the planets and the solid lines mean the planets after 10 giga years. Lines' colors mean the initial intrinsic temperature.

3.4 The dependence on the parameters

In this subsection, we evaluate the dependence on parameters : (1) the initial planet's luminosity $L_{p,0}$, (2) the semi-major axis a, (3) the mass loss efficiency ϵ and (4) the water to rock ratio $X_{w/r}$. In this paper, we define the $M_{\rm thrs}$ as the initial planet's mass whose water composition is evaporated at all after 10 giga years. If the mass loss has strong effects, the $M_{\rm thrs}$ become bigger. We use the threshold mass $M_{\rm thrs}$ to evaluate the sensitivity of parameters; the initial planet's luminosity $L_{p,0}$, the semi-major axis a, the mass loss efficiency ϵ and the initial water to rock ratio $X_{w/r}$.

Some water-rich planets become lager than the Roche lobe in their evolution. If the planet's radius is lager than the Roche lobe, the planet will be experienced the dynamical mass loss. In that case, we consider that the planet becomes the rocky planet and such the case represents the grey dotted-line in the mass-radius diagram.

In fact, the semi-major axis and the mass loss efficiency are not constant values through the planetary lifetime because the planet's situation can change such as orbital evolution. However these problem are beyond the control in this paper.

1. The sensitivity of the initial planet's luminosity $L_{p,0}$

   Figure 5 shows mass-radius relationship taking into account the mass loss of the planet. We change the initial planet's luminosity $10^{23}, 10^{24}, 10^{25}$ and 10^{26} ergs/s and set the semi-major axis $a = 0.05$AU, the water to rock ratio $X_{w/r} = 3$ and the mass loss efficiency $\epsilon = 0.1$ respectively. As $L_{p,0}$ become bigger, the planet's radius become larger at the initial condition. The planet which has larger radius loses more its mass than the smaller one. Therefore, the lager $L_{p,0}$ causes the more mass loss of the planet. If the planet's mass is $\gtrsim 30 M_\oplus$, the mass loss does not have a significant effect on the mass-radius relationship. Because the contraction by the planet's gravity has more efficient than the expansion by the thermal effect for such a high mass planet.

2. The sensitivity of the semi-major axis a

   Figure 6 shows the mass-radius relationship taking into account the mass loss of the planet, taking notice on the difference of the semi-major axis. We change the semi-major axis $0.01, 0.05$ and 0.1 AU and set the initial planet's luminosity $L_{p,0} = 10^{25}$ergs/s, the water to rock ratio $X_{w/r} = 3$ and the mass loss efficiency $\epsilon = 0.1$ respectively. The dotted-lines are the initial states of the planets, solid-lines are the planets whose age are 10 giga year and dashed lines are Roche-lobe radius. If the planet is close to its host star, the planet receive intense irradiation and XUV flux. Moreover the closer planet has the smaller Roche-lobe radius and then $K_{\rm tide}$ becomes smaller, which means $\dot{M}$ become bigger. These two effect make the planet's evaporation strong.

3. The sensitivity of the initial water to rock ratio $X_{w/r}$

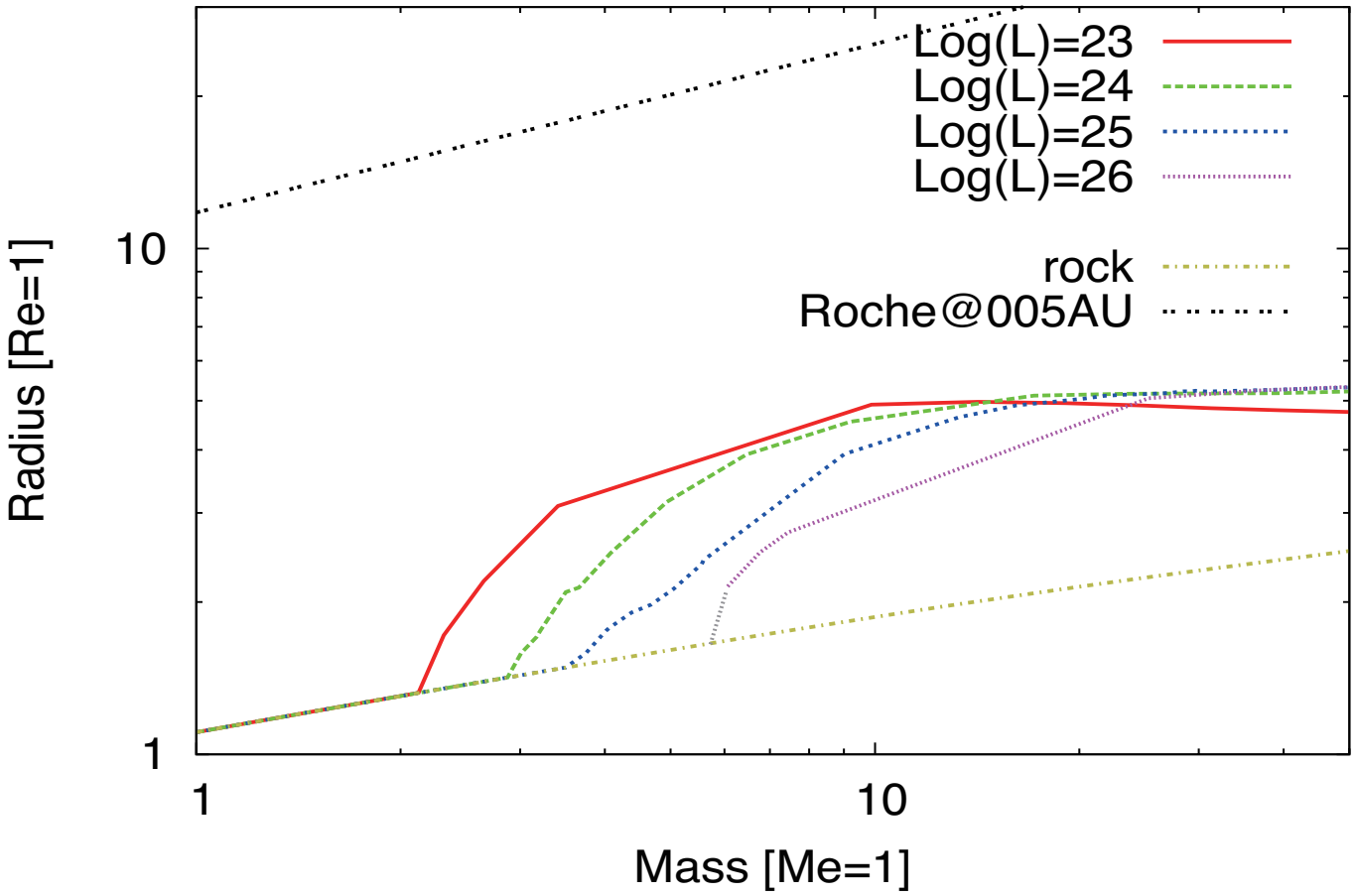

Figure 5: This figure shows the mass-radius relationship of the planets. The x-axis is planets' masses [$M_\oplus$], and the y-axis is planets' radii [$R_\oplus$]. The dotted lines mean the initial state of the planets and the solid lines mean the planets after 10 giga years. Lines' colors mean the initial planet's luminosity; 10^{23}, 10^{24}, 10^{25} and 10^{26}ergs/s respectively.

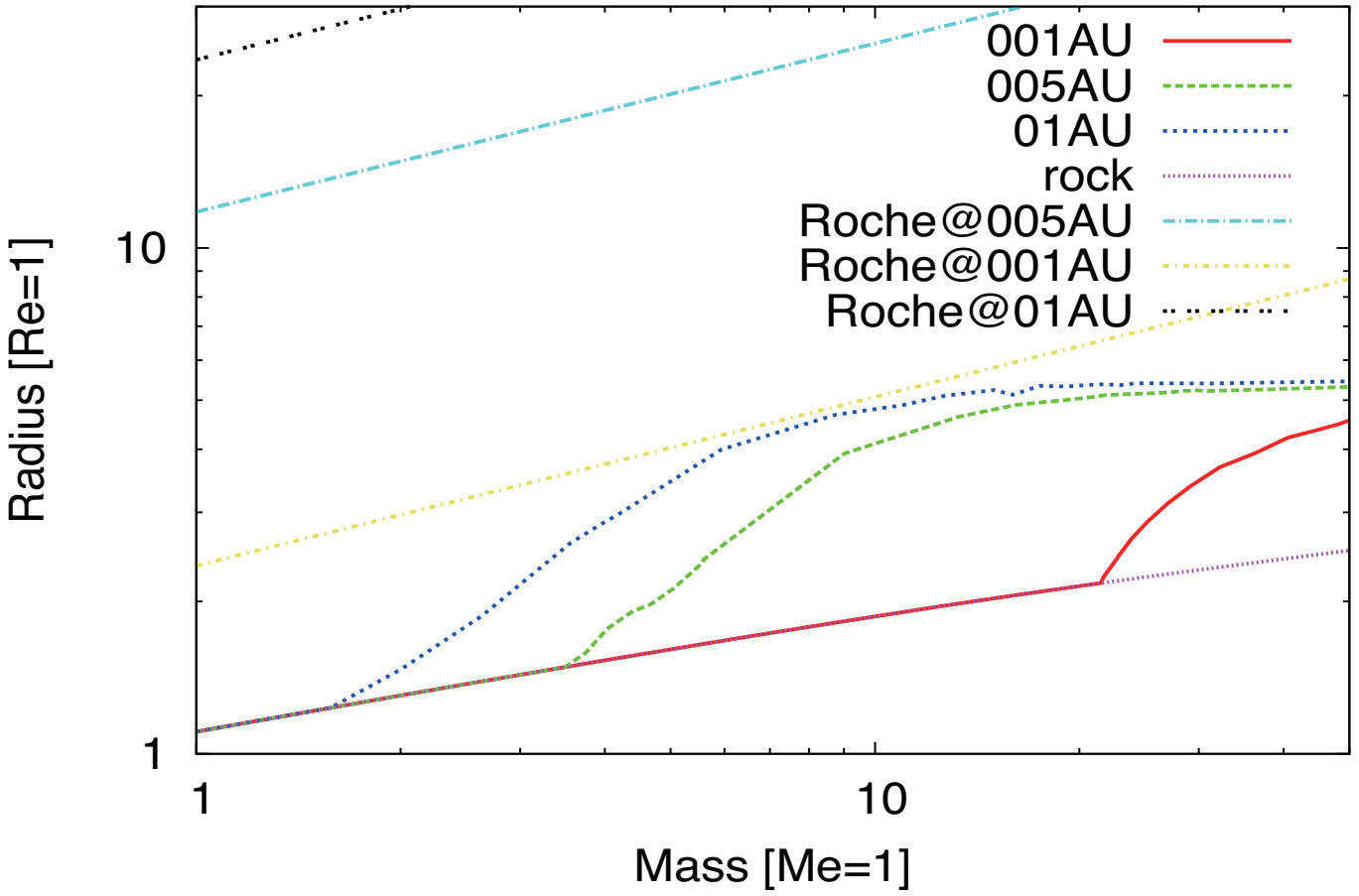

Figure 6: This figure shows the mass-radius relationship of the planets. The x-axis is planets' masses [$M_\oplus$], and the y-axis is planets' radii [$R_\oplus$]. We assume initial planet's luminosity $L_p = 10^{25}$ergs/s, $\epsilon = 0.1$. Colors represent the difference of semi-major axis; 0.01AU (red lines), 0.05AU (blue lines) and 0.1AU (green lines). Dotted lines are the conditions at $t = 0$. Solid lines are the conditions after 10 giga years. Dashed lines are the Roche-lobe radius at 0.05AU.

Figure 7 shows the mass-radius relationship taking notice of the difference of water to rock ratio. We change the water to rock ratio $0.1, 1, 3$ and 10 and set the initial planet's luminosity $L_{p,0} = 10^{25}$ergs/s, the semi-major axis $a = 0.05$AU and the mass loss efficiency $\epsilon = 0.1$ respectively. If the planet's $X_{w/r}$ is small, the planet's composition is dominated by rock. Therefore, the mass loss does not work effective.

4. The sensitivity of the mass loss efficiency ϵ

   Figure 8 shows the mass-radius relationship taking into account the mass loss of the planet, taking notice on the difference of the mass loss efficiency ϵ. We change the mass loss efficiency $0.01, 0.1$ and 1 and set the initial planet's luminosity $L_{p,0} = 10^{25}$ergs/s, the semi-major axis $a = 0.05$AU and the water to rock ratio $X_{w/r} = 3$ respectively. The red-dotted line is the initial state of the planets and gray dotted-line is the Roche-lobe radius. The solid-lines are the planets whose age are 10 giga year. The lines' color, green, blue and purple represent the difference of $\epsilon = 0.01$, 0.1 and 1 respectively. Lager mass loss efficiency causes lager mass loss. On the other hand, when $\epsilon = 0.01$, the planet whose initial state's radius is nearly the Roche-lobe radius remains its water. However, if the planet's radius is lager than the Roche-lobe radius, the planet does not bound its body by own gravity. Hence the planet lose its mass quickly, but in fact our mass loss model does not apply when the planet's radius is lager than the Roche-lobe radius because the planet have experienced non-quasi-static hydrodynamic escape. In Fig.8, the green dotted-line on the green solid-line represent the planets whose radii are lager than the Roche-lobe radius in their evolution.

Here, we summarize $M_{\rm thrs}$ in Table 1

- The initial planet's luminosity $L_{p,0}$

  If we enlarge the $L_{p,0}$ order of magnitude, it makes the $M_{\rm thrs}$ large factor ~ 2.

- The semi-major axis a

  If we change semi-major axis a by 10 times, the $M_{\rm thrs}$ change $\sim$ 10 times. Although the $F_{\rm XUV}$ change as intense as 100 times and the Roche lobe radius changes, the high mass planet tend to contract and sustain mass loss.

- The water to rock ratio $X_{w/r}$

  If we consider the same planet' mass, large $X_{w/r}$ planet tend to inflate and lose its mass more than small $X_{w/r}$ one. The $M_{\rm thrs}$ changes factor ~ 5 between $X_{w/r} = 0.1$ and 10.

- The mass loss efficiency ϵ

  If we enlarge ϵ from 0.01 to 10, $M_{\rm thrs}$ changes factor ~ 3.

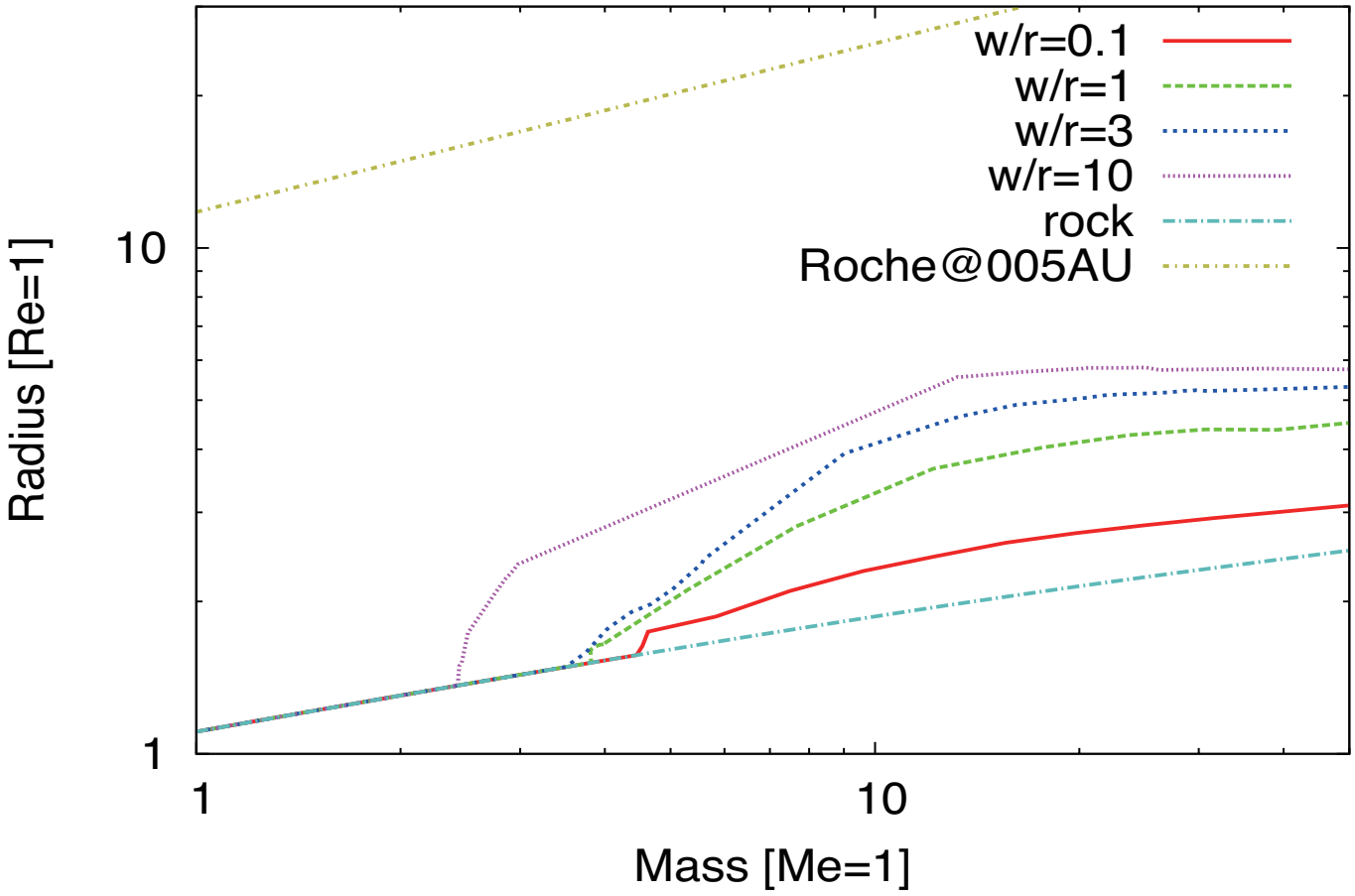

Figure 7: This figure shows the mass-radius relationship of the planets. The x-axis is planets' masses [$M_\oplus$], and the y-axis is planets' radii [$R_\oplus$]. We assume the initial planet's luminosity $L_p = 10^{25}$ergs/s, the semi-major axis $a = 0.05$AU, the mass loss efficiency $\epsilon = 0.1$. Solid lines are the conditions after 10 giga years. We change the water to rock ratio $X_{w/r} = 0.1$ (red line), 1 (green line), 3 (blue line) and 10 (purple line). Dashed line is the Roche-lobe radius.

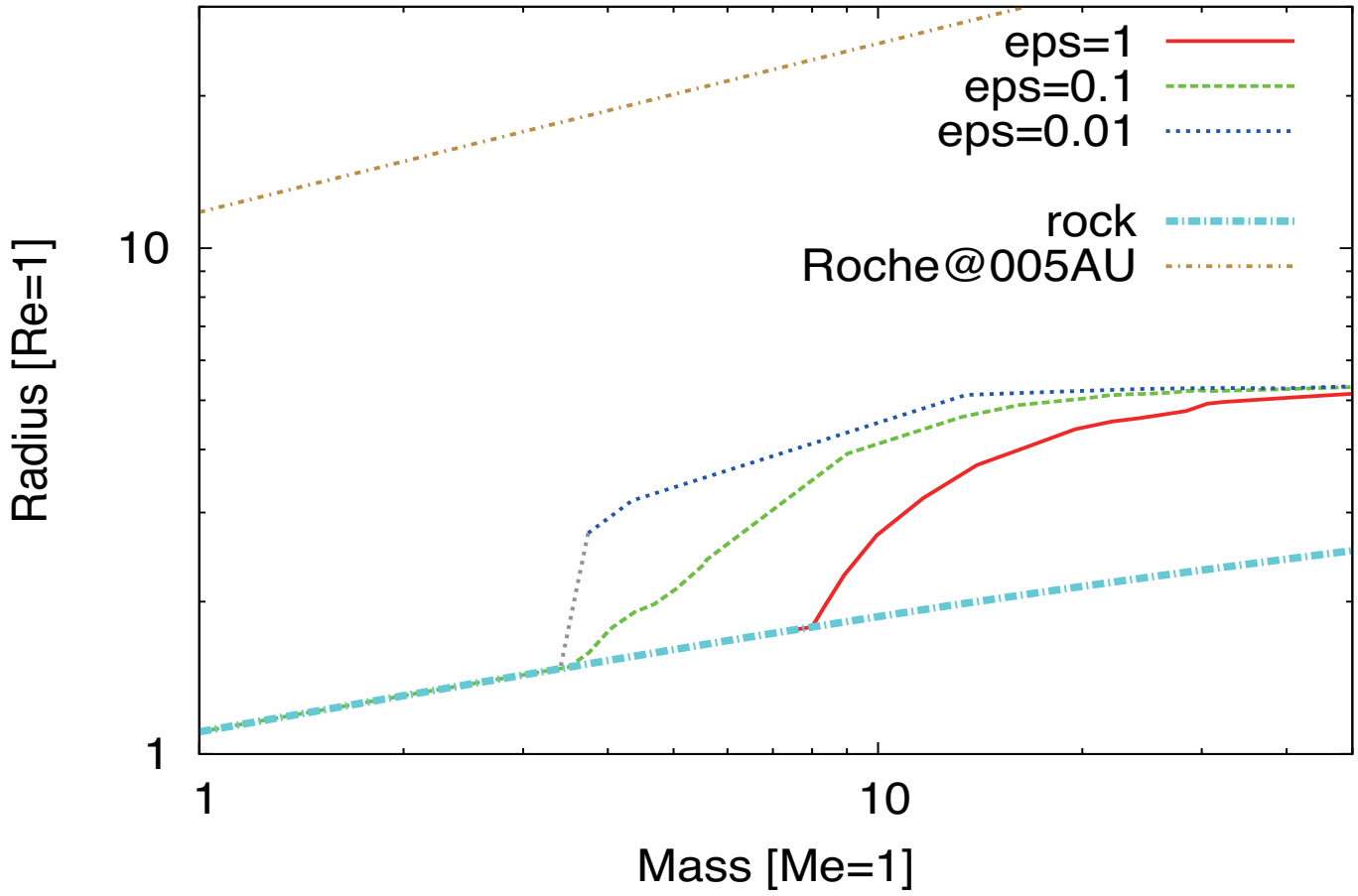

Figure 8: This figure shows the mass-radius relationship of the planets. The x-axis is planets' masses [$M_\oplus$], and the y-axis is planets' radii [$R_\oplus$]. We assume $T_{int,0} = 100$K, $a = 0.05$AU. Colors represent the difference of the mass loss efficiency; 0.01 (green lines), 0.1 (blue lines) and 1 (purple lines). Dotted red line is the conditions at $t = 0$. Solid lines are the conditions after 10 giga years. Dashed line is the Roche-lobe radius.

These results suggest that the mass loss of the planet has a significant effect on the $\sim 10M_\oplus$ planet. Such low mass planet are the transition point between Super-Earths and Hot-Jupiters. Comparing with values of $M_{\rm thrs}$, the semi-major axis a has the largest effect on the mass loss. On the other hand, the initial planet's luminosity $L_{p,0}$ has smaller effect on the mass loss than other parameters.

Table 1: The dependences of parameters of the threshold masses

$L_{p,0}$ [ergs/s]	10^{23}	10^{24}	10^{25}	10^{26}
$M_{\rm thrs}$ $[M_\oplus]$	8.5	11.5	14	23
a[AU]	0.01	0.05	0.1	
$M_{\rm thrs}$ $[M_\oplus]$	86	14	6.3	
$X_{w/r}$	0.1	1	3	10
$M_{\rm thrs}$ $[M_\oplus]$	4.9	7.5	14	26.9
ϵ	0.01	0.1	1	
$M_{\rm thrs}$ $[M_\oplus]$	11.5	14	32	

4 Discussion: implications to the origin

In this section, we discuss implications to the origin of the water-rich planet.

4.1 The giant impact

In this section, we discuss the initial condition of the planet. Here we discuss the planet formed by giant impact.

We calculate the gravitational energy of the planet $E_g(M_p)$ and the impact energy $E_{\rm imp}$;

$$E_{\rm imp} = \frac{1}{2}\mu v_{\rm col}^2, \tag{37}$$

$$v_{\rm imp} = \sqrt{v_{\rm in}^2 + v_{\rm esc}^2 - \frac{2G(m_1+m_2)}{d}}, \tag{38}$$

where $\mu = m_1 m_2/(m_1+m_2)$ that m_1 and m_2 are the impactors' masses, $v_{\rm imp}$ is the impact velocity, $v_{\rm esc}$ is the escape velocity and d is the initial distance between impactors and $v_{\rm in}$ is the relative velocity between impactors when the distance between them is d. We assume $d = 10r_{\rm Hill}$, $v_{\rm in} = ev_{\rm kep}$ (e : the eccentricity, $v_{\rm kep}$: the keplerian velocity) and $M_p = m_1 + m_2$ here. We estimate the planet's gravitational energy after the giant impact,

$$E_g(m_1) + E_g(m_2) + E_{\rm imp} = E_g(M_p). \tag{39}$$

We derive the planet's radius to satisfy the gravitational energy after the giant impact. And we also calculate the thermal evolution and the mass loss over 10 giga years to derive the mass-radius relationship of the water-rich planets.

4.1.1 Numerical results

We adopt the 1 giga years isochron line data as the reference mass, radius and gravitational energy data of the planet. Impactors' masses are m_1, m_2 and their radius are r_1, r_2 respectively.

- In the case of $m_1 = m_2$

  Figure 9 shows the mass-radius relationship in the case of considering the giant impact on $m_1 = m_2$. We assume the eccentricity $e = 0.01$ and the semi-major axis $a = 0.05$AU. If the giant impact event occurs near the host star, the small mass planet will be evaporated at all. That is because the smaller mass planet has the smaller Roche lobe radius.

- In the case of $m_1 = 3m_2$ and $e = 0.01$

  Figure 10 shows the mass-radius relationship in the case of considering the giant impact on $m_1 = 3m_2$. We assume the eccentricity $e = 0.01$ and the semi-major axis $a = 0.05$AU. $M_{\rm thrs}$ of this case is smaller than the case of $m_1 = m_2$. That is because in the case of $m_1 = 3m_2$, the gravitational energy is more deep than the case of $m_1 = m_2$.

- In the case of $m_1 = 3m_2$ and $e = 0.1$

  Figure 11 shows the mass-radius relationship in the case of considering the giant impact on $m_1 = 3m_2$. We assume the eccentricity $e = 0.1$ and the semi-major axis $a = 0.05$AU. $M_{\rm thrs}$ of this case is larger than the case of $e = 0.1$.

We summarize the $M_{\rm thrs}$ for giant impact in Table 2. If we consider $m_2/m_1 = 1$ and $e = 0.1$ then the planet's radius (whose mass is lower than $50M_\oplus$) after the giant impact will be lager than the Roche lobe radius at 0.05AU. Therefore, if the giant impact occur near the host star, the planet will be rocky planet in the case of the impactors' mass fraction ≈ 1 and the high eccentricity $e \approx 0.1$. On the other hand, if the giant impact occur in the case of the impactors' mass fraction is smaller than 1 and the low eccentricity, the planet may keep its water layer.

Table 2: The $M_{\rm thrs}$ for the giant impact

m_2/m_1	e	$M_{\rm thrs}[M_\oplus]$
1	0.01	~ 30
1/3	0.01	~ 15
1/3	0.1	~ 20

4.2 The accretion history of planetesimals

In this section, we discuss the relationship between the initial planet's luminosity and the accretion rate. According to Bodenheimer et al. (1985), the accretion luminosity $L_{\rm acc}$ is

$$L_{\rm acc} = \int_{r_a}^{r_c} -\frac{GM_r}{r^2}\dot{M}dr. \tag{40}$$

We assume the balance of budget between $L_{\rm acc}$ and $L_{p,0}$ is equilibrated, $L_{\rm acc} = L_{p,0}$. And we also assume the accretion radius is equal to the Hill radius and r_c is equal to the planet's radius from center to the radiative-convective interface. We can derive the relationship between $\dot{M}$ and $L_{p,0}$ that

$$\dot{M} = \frac{L_{p,0}}{GM_p\left(R_{\rm conv}^{-1} - r_{\rm Hill}^{-1}\right)}. \tag{41}$$

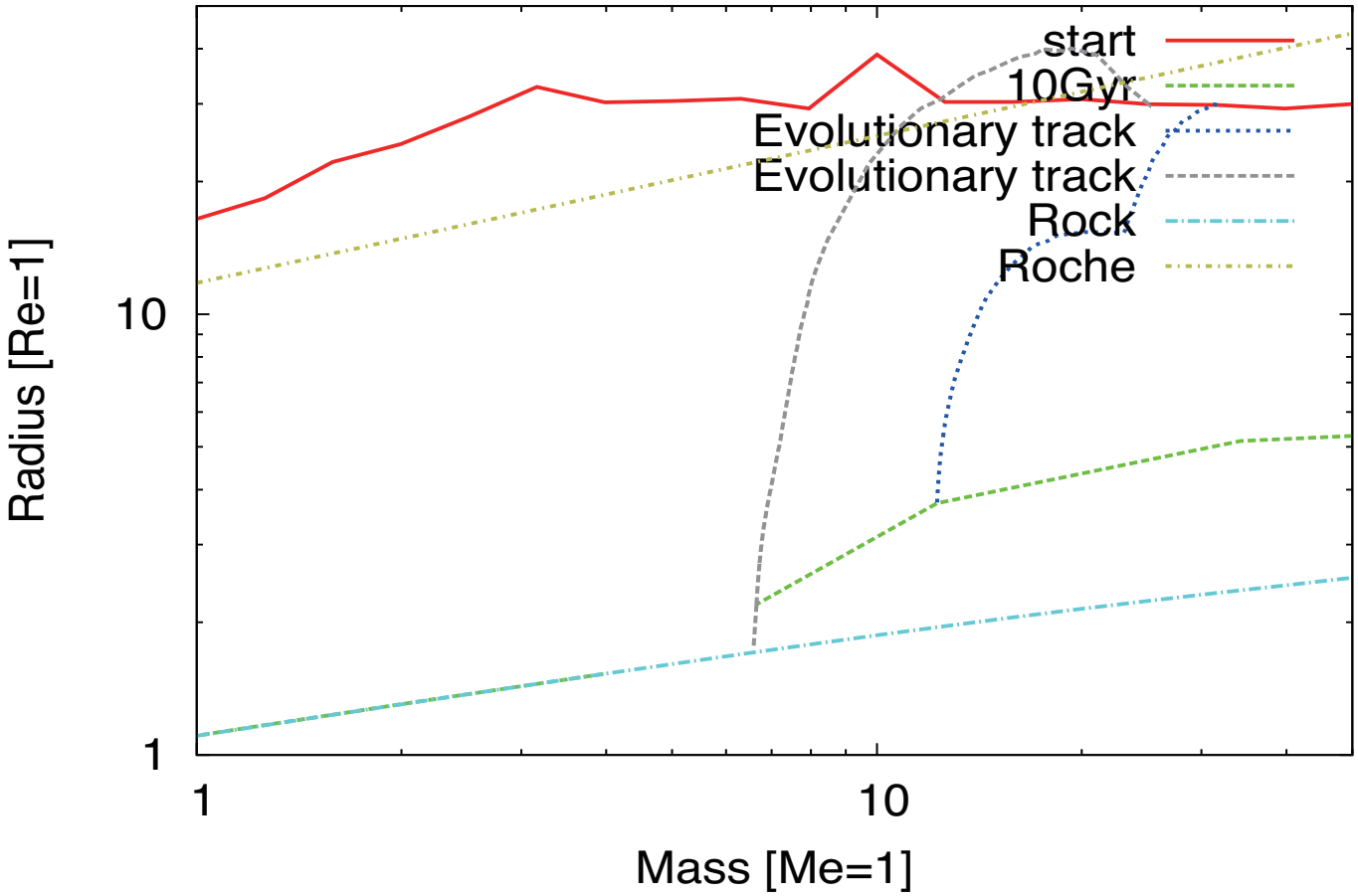

Figure 9: The mass-radius relationship in the case of giant impact. We set the semi-major axis $a = 0.05$AU, the mass loss efficiency $\epsilon = 0.1$, the water to rock ratio $X_{w/r} = 3$. Impactors' mass ratio $m_2/m_1 = 1$ and the eccentricity $e = 0.01$.

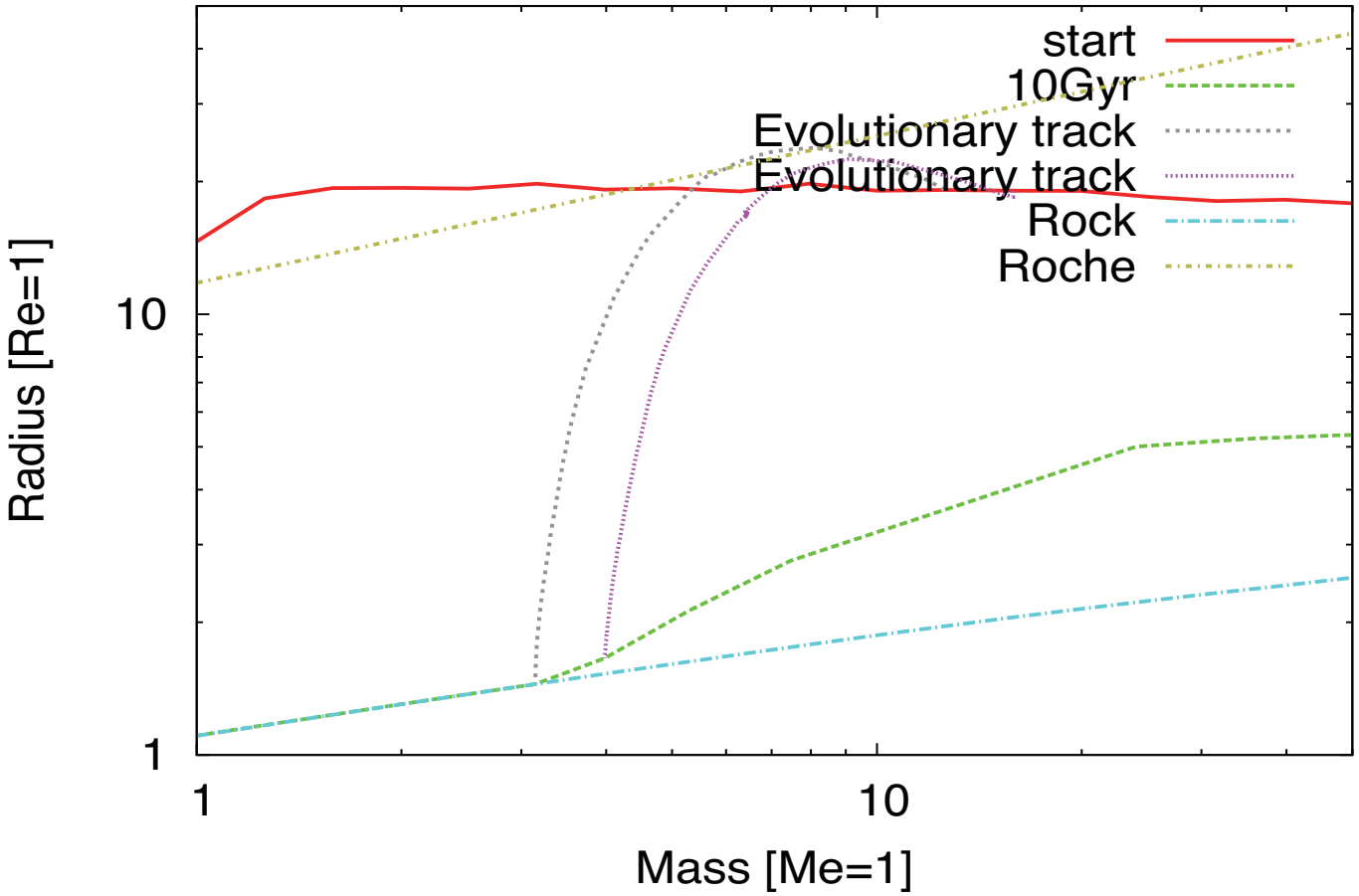

Figure 10: The mass-radius relationship in the case of giant impact. We set the semi-major axis $a = 0.05$AU, the mass loss efficiency $\epsilon = 0.1$, the water to rock ratio $X_{w/r} = 3$. Impactors' mass ratio $m_2/m_1 = 1/3$ and the eccentricity $e = 0.01$.

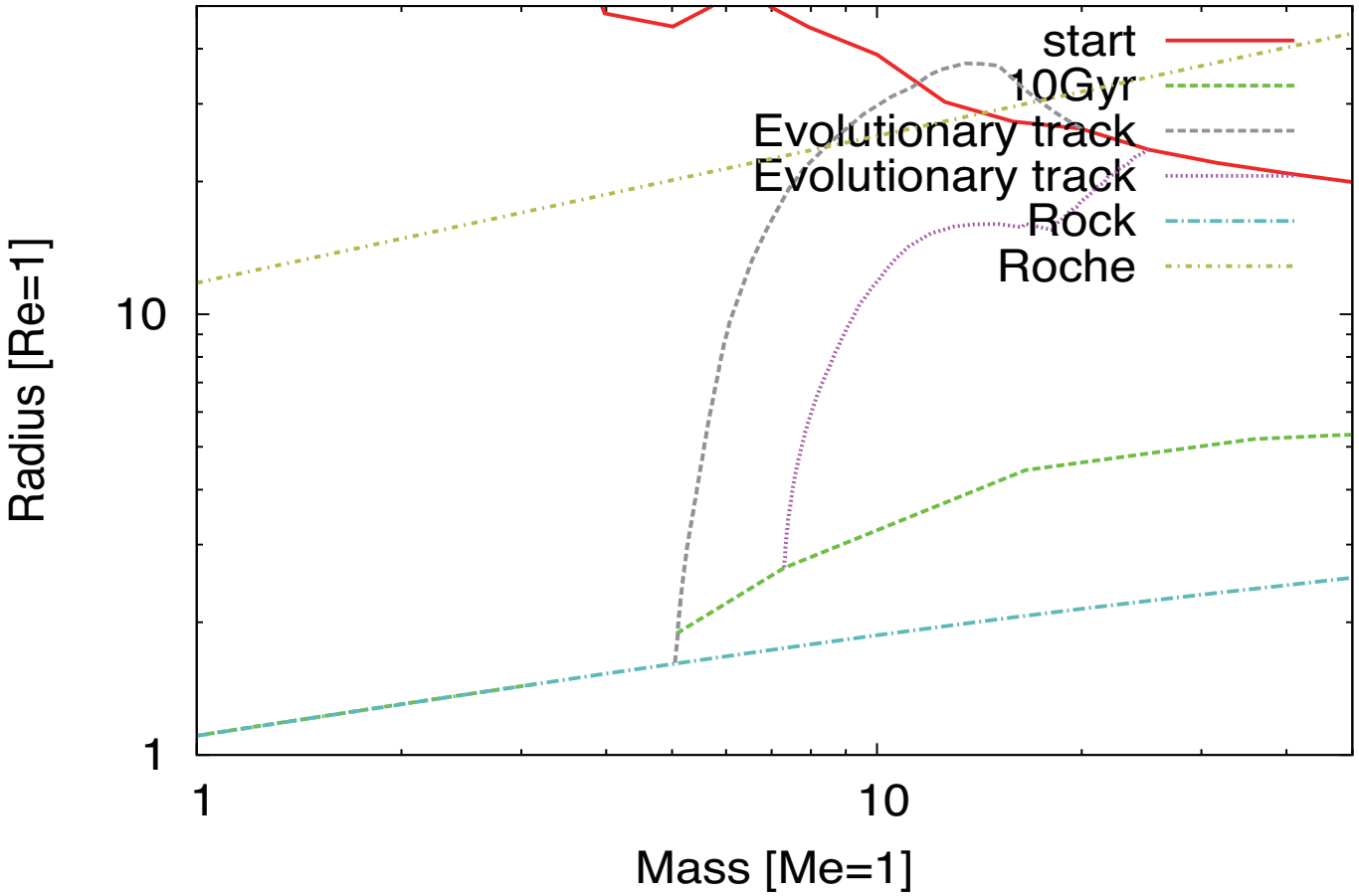

Figure 11: The mass-radius relationship in the case of giant impact. We set the semi-major axis $a = 0.05$AU, the mass loss efficiency $\epsilon = 0.1$, the water to rock ratio $X_{w/r} = 3$. Impactors' mass ratio $m_2/m_1 = 1/3$ and the eccentricity $e = 0.1$.

We summarize results in Table 3. As a result, if $L_{p,0}$ enlarge 10 times, $\dot{M}$ also enlarge 10 times. That is the because the term $\sim GM_p/R_{\rm conv}$ changes only factor times although $L_{p,0}$ changes the order of magnitude. Provided that $R_{\rm conv}^{-1} - r_{\rm Hill}^{-1} \sim R_p$, then we can derive

$$\dot{M} \sim 10^{-7} \left(\frac{L_{p,0}}{10^{25}{\rm ergs/s}} \right) \left(\frac{R_p}{R_\oplus} \right) \left(\frac{M_p}{M_\oplus} \right)^{-1} M_\oplus/{\rm year}, \tag{42}$$

$$\sim 10^{-7} \left(\frac{T_{\rm int}}{4 \times 10^2 {\rm K}} \right)^4 \left(\frac{\bar{\rho}}{\bar{\rho}_\oplus} \right)^{-1} M_\oplus/{\rm year}. \tag{43}$$

This consequence suggests that there is a relationship between the accretion rate $\dot{M}$ and the initial condition of the planet, especially its environment of the surface.

Table 3: The relationship among the initial planet's luminosity $L_{p,0}$, the threshold mass $M_{\rm thrs}$ and the accretion rate $\dot{M}$

$L_{p,0}$ [ergs/s]	$M_{\rm thrs}[M_\oplus]$	$R_p(M_{\rm thrs}, L_{p,0})[R_\oplus]$	$\dot{M}[M_\oplus/{\rm year}]$
10^{23}	8.5	7.79	1.0×10^{-9}
10^{24}	11.5	11.2	1.2×10^{-8}
10^{25}	14	18.3	2.5×10^{-7}
10^{26}	23	23.5	2.4×10^{-6}

5 Conclusion

We derive water-rich planets' mass-radius relation in the two case:

- Neglect the effect of mass loss (see Fig.2).
- Include the effect of mass loss (see Fig.4).

Figure 2 shows that the effect of only shrinkage by cooling dose not enough to explain observations. If the water to rock ratio is bigger, the planets' radius become lager because water component become dominant.

The mass loss has significant effect on the planet's mass-radius relationship especially low-mass planets. Low-mass planets lose their water layer and become the water-poor or rocky planet.

References

[1] Adams, E. R., Seager, S., & Elkins-Tanton, L. 2008, apj, 673, 1160

[2] Baraffe, I., Chabrier, G., Barman, T. S., Allard, F., & Hauschildt, P. H. 2003, aap, 402, 701

[3] Baraffe, I., Selsis, F., Chabrier, G., et al. 2004, aap, 419, L13

[4] Baraffe, I., Chabrier, G., Barman, T. S., et al. 2005, aap,436, L47

[5] Baraffe, I., Alibert, Y., Chabrier, G., & Benz, W. 2006, aap450, 1221

[6] Baraffe, I., Chabrier, G., & Barman, T. 2008, aap482, 315

[7] Bean, J. L., Miller-Ricci Kempton, E., & Homeier, D. 2010, nat,468, 669

[8] Bean, J. L., Désert, J.-M., Kabath, P., et al. 2011, apj743, 92

[9] Bodenheimer, P. 1985, Protostars and Planets II, 873

[10] Croll, B., Albert, L., Jayawardhana, R., et al. 2011, apj736, 78

[11] Crossfield, I. J. M., Barman, T., & Hansen, B. M. S. 2011, apj736, 132

[12] Désert, J.-M., Bean, J., Miller-Ricci Kempton, E., et al. 2011, apjl731, L40

[13] Ehrenreich, D., & Désert, J.-M. 2011, aap529, A136

[14] Erkaev, N. V., Kulikov, Y. N., Lammer, H., et al. 2007, aap, 472, 329

[15] Fortney, J. J., & Marley, M. S. 2007, apjl, 666, L45

[16] Fortney, J. J., Marley, M. S., & Barnes, J. W. 2007, apj, 659, 1661

[17] Fortney, J. J., Marley, M. S., & Barnes, J. W. 2007, apj, 668, 1267

[18] Fortney, J. J., & Nettelmann, N. 2010, ssr, 152, 423

[19] Fortney, J. J., Baraffe, I., & Militzer, B. 2011, Exoplanets, edited by S. Seager. Tucson, AZ: University of Arizona Press, 2011, 526 pp. ISBN 978-0-8165-2945-2., p.397-418, 397

[20] Fortney, J. J., Ikoma, M., Nettelmann, N., Guillot, T., & Marley, M. S. 2011, apj, 729, 32

[21] Grasset, O., Schneider, J., & Sotin, C. 2009, apj, 693, 722

[22] Guillot, T., Gautier, D., Chabrier, G., & Mosser, B. 1994, icarus, 112, 337

[23] Guillot, T., Chabrier, G., Morel, P., & Gautier, D. 1994, icarus, 112, 354

[24] Guillot, T., Chabrier, G., Gautier, D., & Morel, P. 1995, apj, 450, 463

[25] Guillot, T., Burrows, A., Hubbard, W. B., Lunine, J. I., & Saumon, D. 1996, apjl, 459, L35

[26] Guillot, T. 1999, Science, 286, 72

[27] Guillot, T. 2005, Annual Review of Earth and Planetary Sciences, 33, 493

[28] Guillot, T. 2010, aap, 520, A27

[29] Hansen, B. M. S. 2008, apjs, 179, 484

[30] Heng, K., Hayek, W., Pont, F., & Sing, D. K. 2012, mnras, 420, 20

[31] Hubbard, W. B., & Macfarlane, J. J. 1980, jgr, 85, 225

[32] Hubbard, W. B., & Marley, M. S. 1989, icarus,78, 102

[33] Hubbard, W. B., Podolak, M., & Stevenson, D. J. 1995, Neptune and Triton, 109

[34] Ikoma, M., Nakazawa, K., & Emori, H. 2000, apj, 537, 1013

[35] Ikoma, M., & Genda, H. 2006, apj, 648, 696

[36] Ikoma, M., & Hori, Y. 2012, apj, 753, 66

[37] Kippenhahn, R., & Weigert, A. 1990, Stellar Structure and Evolution, XVI, 468 pp. 192 figs.. Springer-Verlag Berlin Heidelberg New York. Also Astronomy and Astrophysics Library,

[38] Léger, A., Selsis, F., Sotin, C., et al. 2004, icarus169, 499

[39] Lecavelier des Etangs, A., Vidal-Madjar, A., McConnell, J. C., & Hébrard, G. 2004, aap, 418, L1

[40] Lecavelier Des Etangs, A., & Vidal-Madjar, A. 2005, Protostars and Planets V, 8050

[41] Lecavelier Des Etangs, A. 2007, aap, 461, 1185

[42] Lecavelier Des Etangs, A., Ehrenreich, D., Vidal-Madjar, A., et al. 2010, aap, 514, A72

[43] Lyon, S. & Johnson, J. D. e. 1992, SESAME: Los Alamos National Laboratory Equation of State Database, Tech, rep., LANL report no. LA-UR-92-3407

[44] Murray-Clay, R. A., Chiang, E. I., & Murray, N. 2009, apj, 693, 23

[45] Nettelmann, N., Kramm, U., Redmer, R., & Neuhäuser, R. 2010, aap, 523, A26

[46] Nettelmann, N., Fortney, J. J., Kramm, U., & Redmer, R. 2011, apj, 733, 2

[47] Podolak, M., Weizman, A., & Marley, M. 1995, planss, 43, 1517

[48] Ribas, I., Guinan, E. F., Güdel, M., & Audard, M. 2005, apj, 622, 680

[49] Sanz-Forcada, J., Ribas, I., Micela, G., et al. 2010, aap, 511, L8

[50] Sanz-Forcada, J., Ribas, I., Micela, G., et al. 2010, aap, 520, 1

[51] Sanz-Forcada, J., Micela, G., Ribas, I., et al. 2011, aap, 532, A6

[52] Rogers, L. A., & Seager, S. 2010, apj, 712, 974

[53] Rogers, L. A., & Seager, S. 2010, apj, 716, 1208

[54] Rogers, L. A., Bodenheimer, P., Lissauer, J. J., & Seager, S. 2011, apj, 738, 59

[55] Rothman, L. S., Gamache, R. R., Tipping, R. H., et al. 1992, jqsrt,48, 469

[56] Seager, S., Kuchner, M., Hier-Majumder, C. A., & Militzer, B. 2007, apj, 669, 1279

[57] Sekiya, M., Nakazawa, K., & Hayashi, C. 1980, Progress of Theoretical Physics, 64, 1968

[58] Sotin, C., Grasset, O., & Mocquet, A. 2007, icarus, 191, 337

[59] Stevenson, D. J. 1982, Annual Review of Earth and Planetary Sciences, 10, 257

[60] Valencia, D., O'Connell, R. J., & Sasselov, D. 2006, icarus, 181, 545

[61] Valencia, D., Sasselov, D. D., & O'Connell, R. J. 2007, apj, 656, 545

[62] Valencia, D., Ikoma, M., Guillot, T., & Nettelmann, N. 2010, aap, 516, A20

[63] Vidal-Madjar, A., Lecavelier des Etangs, A., Désert, J.-M., et al. 2003, nat, 422, 143

[64] Vidal-Madjar, A., Désert, J.-M., Lecavelier des Etangs, A., et al. 2004, apjl, 604, L69

[65] Watson, A. J., Donahue, T. M., & Walker, J. C. G. 1981, icarus, 48, 150

[66] Yelle, R. V. 2004, icarus, 170, 167

[67] Yelle, R. V. 2006, icarus, 183, 508

[68] Yelle, R., Lammer, H., & Ip, W.-H. 2008, ssr, 139, 437

[69] Zapolsky, H. S., & Salpeter, E. E. 1969, apj,158, 809

A Analytical formula of the mass loss

We derive the analytical formula of the water-rich planet's escaped mass $M_{\rm esc}$. According to Valencia et al. (2010), the planet's mean density $r\bar{h}o$ is constant through the evolution,

$$\begin{aligned}\dot{M} &= 9.0\times10^{10} \\ &\times\left(\frac{\epsilon}{0.1}\right)\left(\frac{K_{\rm tide}}{0.8}\right)^{-1}\left(\frac{\bar{\rho}}{1{\rm g/cm^2}}\right)^{-1}\left(\frac{a}{0.05{\rm AU}}\right)^{-2}{\rm g/s}\end{aligned} \tag{44}$$

for $t < 0.1$Gyr and

$$\begin{aligned}\dot{M} &= 5.3\times10^{9}\left(\frac{\epsilon}{0.1}\right)\left(\frac{K_{\rm tide}}{0.8}\right)^{-1} \\ &\times\left(\frac{\bar{\rho}}{1{\rm g/cm^2}}\right)^{-1}\left(\frac{a}{0.05{\rm AU}}\right)^{-2}\left(\frac{t}{1{\rm Gyr}}\right)^{-1.23}{\rm g/s}\end{aligned} \tag{45}$$

for $t \geq 0.1$Gyr.

Generally, the lower mass planet have the lower mean density than the higher one because of the effect of gravitational compression. We assume the simple power law relation between the planet's mean density and planet's mass;

$$\bar{\rho} = \rho_0\left(\frac{M_p}{M_N}\right)^k. \tag{46}$$

where M_p is the planet's mass and M_N is the Neptune mass ($M_N = 17.1471 M_\oplus$). We also take into account the shrinkage of the planet's radius by cooling. We assume it is simply described by the power law;

$$t < \tau_{\rm KH,0} \implies R = R_0, \tag{47}$$

$$t \geq \tau_{\rm KH,0} \implies R = R_0\left(\frac{t}{\tau_{\rm KH,0}}\right)^{-l}, \tag{48}$$

where t is time, R_0 is the planet's initial radius, and $\tau_{\rm KH,0}$ is the Kelvin-Helmholtz timescale at the initial condition of the planet; $\tau_{\rm KH,0} = GM_p^2/(2R_0L_{p,0})$, where $L_{p,0} = 4\pi R_0^2\sigma T_{\rm int,0}^4$.

The XUV flux irradiated from the host star is

$$t < t_0 \implies F_{\rm XUV} = A_0\left(\frac{a}{1{\rm AU}}\right)^{-2}, \tag{49}$$

$$t \geq t_0 \implies F_{\rm XUV} = A\left(\frac{t}{1{\rm Gyr}}\right)^{\alpha}\left(\frac{a}{1{\rm AU}}\right)^{-2}, \tag{50}$$

where $A_0 = A(t_0/1\mathrm{Gyr})^\alpha$.

If we assume the mass loss is worked only by $F_{\rm XUV}$ from the host star, the mass loss stars when the protoplanetary disk has been disappeared. Here, we set the time scale of disappearing the disk τ_d. Then, we can find

$$t < \tau_d \implies \dot{M} = 0, \tag{51}$$

$$t \geq \tau_d \implies \dot{M} = -\frac{3\epsilon}{4GK_{\rm tide}}\frac{F_{\rm XUV}}{\bar{\rho}}. \tag{52}$$

Here, we summarize assumptions to derive the analytical formula:

1. We assume the planet's mean density $\bar{\rho}$;

$$\bar{\rho}(t) = \rho_0 \left(\frac{M(t)}{M_N}\right)^k \left(\frac{t}{\tau_{\rm KH,0}}\right)^{3l}. \tag{53}$$

   where the power law coefficients k and l are constant through the evolution.

2. The planet's radius R_p is constant until the planet's age reaches $\tau_{\rm KH,0}$; $t < \tau_{\rm KH,0} \implies R_p = \mathrm{Const.}$
3. The depletion of the $F_{\rm XUV}$ starts from t_0.
4. The $F_{\rm XUV}$ begins to decrease after the planetary disk has dissipated; $t_0 > \tau_d$
5. The mass loss starts when the protoplanetary disk has dissipated : $t = \tau_d$.
6. The mass loss efficiency ϵ, the compensation term by the tidal effect $K_{\rm tide}$ and the semi-major axis a are constant through the evolution.

Note that there are two kinds of origins of planets. One is the hot start planet and the other is the cold start planet. The cold start planet's $\tau_{\rm KH,0}$ can be longer than τ_d. Here, we part the case of $\tau_{\rm KH,0} \leq \tau_d$ as the hot start planet and the case of $\tau_{\rm KH,0} > \tau_d$ as the cold start planet.

A.1 The hot start planet

In the case of the hot start planet, we integrate $\dot{M}$ by three periods for $[0, \tau_d], [\tau_d, t_0]$ and $[t_0, t]$. Therefore we can find that $[0, \tau_d]$ is

$$M(\tau_d) - M(0) = 0, \tag{54}$$

and $[\tau_d, t_0]$ is

$$\left(\frac{M(t_0)}{M_N}\right)^{k+1} - \left(\frac{M(\tau_d)}{M_N}\right)^{k+1} = \frac{C_H}{1-3l}\left\{t_0\left(\frac{t_0}{\tau_d}\right)^{-3l} - \tau_d\right\}, \tag{55}$$

and $[t_0, t]$ is

$$\begin{aligned} & \left(\frac{M(t)}{M_N}\right)^{k+1} - \left(\frac{M(t_0)}{M_N}\right)^{k+1} \\ = & \frac{C_H}{1+\alpha-3l}\left\{t\left(\frac{t}{t_0}\right)^{\alpha}\left(\frac{t}{\tau_d}\right)^{-3l} - t_0\left(\frac{t_0}{\tau_d}\right)^{-3l}\right\}, \end{aligned} \tag{56}$$

where

$$C_H = -\frac{3\epsilon A(1+k)}{4GK_{\rm tide}M_N}\left\{\rho_0\left(\frac{\tau_d}{\tau_{\rm KH,0}}\right)^{3l}\right\}^{-1}\left(\frac{a}{1{\rm AU}}\right)^{-2}\left(\frac{t_0}{1{\rm Gyr}}\right)^{\alpha}. \tag{57}$$

We sum up (54), (55) and (56) and then we can find

$$\left(\frac{M(t)}{M_N}\right)^{k+1} - \left(\frac{M(0)}{M_N}\right)^{k+1} = C_H D_H, \tag{58}$$

where

$$\begin{aligned} D_H = & \frac{1}{1-3l}\left\{t_0\left(\frac{t_0}{\tau_d}\right)^{-3l} - \tau_d\right\} \\ & + \frac{1}{1+\alpha-3l}\left\{t\left(\frac{t}{t_0}\right)^{\alpha}\left(\frac{t}{\tau_d}\right)^{-3l} - t_0\left(\frac{t_0}{\tau_d}\right)^{-3l}\right\} \end{aligned} \tag{59}$$

In fact, $\rho_0(\tau_d/\tau_{\rm KH,0})^{3l}$ in (57) is the planet's mean density when the disk has been disappeared. If the planet's formation follows the "hot start" scenario, the disk depletion time scale limits the planet's mass loss.

A.2 The cold start planet

In the case of the cold start planet, we integrate $\dot{M}$ by four periods for $[0, \tau_d]$, $[\tau_d, \tau_{\rm KH,0}]$, $[\tau_{\rm KH,0}, t_0]$ and $[t_0, t]$. Therefore we can find that $[0, \tau_d]$ is

$$M(\tau_d) - M(0) = 0 \tag{60}$$

and $[\tau_d, \tau_{\rm KH,0}]$ is

$$\left(\frac{M(\tau_{\rm KH,0})}{M_N}\right)^{k+1} - \left(\frac{M(\tau_d)}{M_N}\right)^{k+1} = C_C\left(\tau_{\rm KH,0} - \tau_d\right) \tag{61}$$

and $[\tau_{\rm KH,0}, t_0]$ is

$$\left(\frac{M(t_0)}{M_N}\right)^{k+1} - \left(\frac{M(\tau_{\rm KH,0})}{M_N}\right)^{k+1} = \frac{C_C}{1-3l}\left\{t_0\left(\frac{t_0}{\tau_{\rm KH,0}}\right)^{-3l} - \tau_{\rm KH,0}\right\}, \quad (62)$$

and $[t_0, t]$ is

$$\begin{aligned}&\left(\frac{M(t)}{M_N}\right)^{k+1} - \left(\frac{M(t_0)}{M_N}\right)^{k+1} \\ =\ & \frac{C_C}{1+\alpha-3l}\left\{t\left(\frac{t}{t_0}\right)^{\alpha}\left(\frac{t}{\tau_{\rm KH,0}}\right)^{-3l} - t_0\left(\frac{t_0}{\tau_{\rm KH,0}}\right)^{-3l}\right\}, \end{aligned} \quad (63)$$

where

$$C_C = -\frac{3\epsilon A(1+k)}{4GK_{\rm tide}M_N}\frac{1}{\rho_0}\left(\frac{a}{1{\rm AU}}\right)^{-2}\left(\frac{t_0}{1{\rm Gyr}}\right)^{\alpha}. \quad (64)$$

We sum up (60), (61), (62) and (63) and then we can find

$$\left(\frac{M(t)}{M_N}\right)^{k+1} - \left(\frac{M(0)}{M_N}\right)^{k+1} = C_C D_C \quad (65)$$

where

$$\begin{aligned} D_C =\ & (\tau_{\rm KH,0} - \tau_d) \\ & + \frac{1}{1-3l}\left\{t_0\left(\frac{t_0}{\tau_{\rm KH,0}}\right)^{-3l} - \tau_{\rm KH,0}\right\} \\ & \frac{1}{1+\alpha-3l}\left\{t\left(\frac{t}{t_0}\right)^{\alpha}\left(\frac{t}{\tau_{\rm KH,0}}\right)^{-3l} - t_0\left(\frac{t_0}{\tau_{\rm KH,0}}\right)^{-3l}\right\}. \end{aligned} \quad (66)$$

A.3 In the case of the low initial luminosity : $\tau_d < t_0 < \tau_{\rm KH,0}$

In the case of $\tau_d < t_0 < \tau_{\rm KH,0}$, we integrate $\dot{M}$ by four periods for $[0, \tau_d]$, $[\tau_d, t_0]$, $[t_0, \tau_{\rm KH,0}]$ and $[\tau_{\rm KH,0}, t]$. Therefore we can find that $[0, \tau_d]$ is

$$M(\tau_d) - M(0) = 0 \quad (67)$$

and $[\tau_d, t_0]$ is

$$\left(\frac{M(t_0)}{M_N}\right)^{k+1} - \left(\frac{M(\tau_d)}{M_N}\right)^{k+1} = C_L\left(t_0 - \tau_d\right) \quad (68)$$

and $[t_0, \tau_{\rm KH,0}]$ is

$$\left(\frac{M(\tau_{\rm KH,0})}{M_N}\right)^{k+1} - \left(\frac{M(t_0)}{M_N}\right)^{k+1} = \frac{C_L}{1+\alpha}\left\{\tau_{\rm KH,0}\left(\frac{\tau_{\rm KH,0}}{t_0}\right)^{\alpha} - t_0\right\}, \quad (69)$$

and $[\tau_{\rm KH,0}, t]$ is

$$\begin{aligned}&\left(\frac{M(t)}{M_N}\right)^{k+1} - \left(\frac{M(\tau_{\rm KH,0})}{M_N}\right)^{k+1} \\ =\ & \frac{C_L}{1+\alpha-3l}\left\{t\left(\frac{t}{t_0}\right)^{\alpha}\left(\frac{t}{\tau_{\rm KH,0}}\right)^{-3l} - \tau_{\rm KH,0}\left(\frac{\tau_{\rm KH,0}}{t_0}\right)^{\alpha}\right\}, \end{aligned} \quad (70)$$

where

$$C_L = -\frac{3\epsilon A(1+k)}{4GK_{\rm tide}M_N}\frac{1}{\rho_0}\left(\frac{a}{1{\rm AU}}\right)^{-2}\left(\frac{t_0}{1{\rm Gyr}}\right)^{\alpha}. \quad (71)$$

We sum up (67), (68), (69) and (70) and then we can find

$$\left(\frac{M(t)}{M_N}\right)^{k+1} - \left(\frac{M(0)}{M_N}\right)^{k+1} = C_L D_L \quad (72)$$

where

$$\begin{aligned} D_L =\ & (t_0 - \tau_d) \\ & + \frac{1}{1+\alpha}\left\{\tau_{\rm KH,0}\left(\frac{\tau_{\rm KH,0}}{t_0}\right)^{\alpha} - t_0\right\} \\ & + \frac{1}{1+\alpha-3l}\left\{t\left(\frac{t}{t_0}\right)^{\alpha}\left(\frac{t}{\tau_{\rm KH,0}}\right)^{-3l} - \tau_{\rm KH,0}\left(\frac{\tau_{\rm KH,0}}{t_0}\right)^{\alpha}\right\} \end{aligned} \quad (73)$$

A.4 Estimate the threshold mass $M_{\rm thrs}$

Provided that we use the parameters which we use in this work. In our calculation, our water-rich planet's mean density is

$$\bar{\rho} = 3\times10^{-2}\left(\frac{M_p}{M_N}\right)^{1}\left(\frac{t}{5\times10^7{\rm years}}\right)^{0.6}. \quad (74)$$

when we assume $L_{p,0} \approx 10^{25}{\rm erg/(s{\cdot}cm^2)}$, $a = 0.05{\rm AU}$ and $X_{w_r} = 3$. In the case of the hot start, we can obtain

$$\begin{aligned} C_H =\ & -5.2\times10^{-16} \\ & \times\left(\frac{\epsilon}{0.1}\right)\left(\frac{A}{29.7{\rm erg/(s\cdot cm^2)}}\right)\left(\frac{1+k}{2}\right)\left(\frac{K_{\rm tide}}{0.8}\right)^{-1} \\ & \times\left(\frac{\rho_0}{0.01{\rm g/cm^3}}\right)^{-1}\left(\frac{a}{0.05{\rm AU}}\right)^{-2}\left(\frac{t_0}{0.1{\rm Gyr}}\right)^{-1.23}. \end{aligned} \quad (75)$$

We set $\tau_d = 10^7$years, $t_0 = 10^8$years and $t = 10^{10}$years. Then we can obtain

$$D_H = 2.1 \times 10^{15}. \tag{76}$$

If $M(t = 10^{10}\text{years}) = 0$ and $k = 1$, we can obtain the threshold mass

$$M_{\rm thrs} = 1.1 M_N = 18 M_\oplus. \tag{77}$$

In the case of the cold start, we can obtain

$$\begin{aligned} C_C &= -1.7 \times 10^{-16} \\ &\times \left(\frac{\epsilon}{0.1}\right) \left(\frac{A}{29.7\text{erg}/(\text{s}\cdot\text{cm}^2)}\right) \left(\frac{1+k}{2}\right) \left(\frac{K_{\rm tide}}{0.8}\right)^{-1} \\ &\times \left(\frac{\rho_0}{0.03\text{g}/\text{cm}^3}\right)^{-1} \left(\frac{a}{0.05\text{AU}}\right)^{-2} \left(\frac{t_0}{0.1\text{Gyr}}\right)^{-1.23}. \end{aligned} \tag{78}$$

We set $\tau_{\rm KH,0} = 5 \times 10^7$years, $\tau_d = 10^7$years, $t_0 = 10^8$years and $t = 10^{10}$years. Then we can obtain

$$D_C = 5.0 \times 10^{15} \tag{79}$$

If $M(t = 10^{10}\text{years}) = 0$ and $k = 1$, we can obtain the threshold mass

$$M_{\rm thrs} = 0.93 M_N = 16 M_\oplus. \tag{80}$$

On the other hand, if we apply the formula derived by Valencia et al. (2010), we can obtain the threshold mass

$$M_{\rm thrs} = 5.3 M_\oplus \tag{81}$$

for $\rho_0 = 0.1\text{g}/\text{cm}^3$, which is the water-rich planet's mean density at $t \sim 10^9$years. Comparing with our numerical result, our formula is more accurate than the pioneering work. Note that these formula do not apply if the planet's composition significantly varies. If the planet's composition has vary, the planet's mean density profile must change. In that case we have to calculate by numerical solution. In fact, the time evolution of the water to rock ratio $X_{w/r}$ has large effect on the $M_{\rm thrs}$ value. If the rocky component become rich, the planet's radius tend to shrink. and then the effect of mass loss becomes small. This effect causes that $M_{\rm thrs}$ derived by our analytical formula is larger than $M_{\rm thrs}$ derived by our numerical study.

B Analytical formula of the giant impact

We consider the giant impact event as two impactors having a collide each other. Here we call the higher mass impactor "1", the lower mass impactor "2" and the planet made by the two impactors' collision "3". $m_i (i = 1, 2, 3)$ represent planets' masses and $r_i (i = 1, 2, 3)$ represent planets' radii. We assume $m_3 = m_1 + m_2$. The gravitational energy represent $E_g(m_i) = -\zeta_i G m_i^2 / r_i$. We use $v_{\rm imp} \approx \sqrt{v_{\rm in}^2 + v_{\rm esc}^2}$, where $v_{\rm in}$ is typically $\sim e v_{\rm Kep}$. And we also use $m_2/m_1 = \gamma_m (\leq 1)$ and $r_2/r_1 = \gamma_r$. Then we can derive

$$E_g(m_3) = \left[\left(1 + \frac{\zeta_2}{\zeta_1} \frac{\gamma_m^2}{\gamma_r} \right) - \frac{\gamma_m}{\zeta_1 (1 + \gamma_m)} \left\{ \frac{1 + \gamma_m}{1 + \gamma_r} + \left(\frac{v_{\rm in}}{v_{\rm esc,1}} \right)^2 \right\} \right] E_g(m_1) \tag{82}$$

where $v_{\rm esc,1} = \sqrt{2 G m_1 / r_1}$.

ζ_i is typically ~ 1. As the planet's mass become large or cool, ζ_i become small. Therefore we can find $\zeta_2 \geq \zeta_1$ if the planet's age is the same.

(82) suggests the requirement to be united after the collision. If $v_{\rm in}$ satisfy the condition;

$$v_{\rm in} \geq v_{\rm esc,1} \sqrt{ \left(1 + \frac{1}{\gamma_m} \right) \left(\zeta_1 + \frac{\gamma_m^2}{\gamma_r} \zeta_2 - \frac{\gamma_m}{1 + \gamma_r} \right) }, \tag{83}$$

the planet cannot be bound to its gravity because of $E_g(m_3) \geq 0$. For example, in the case of $m_1 = m_2$, we can derive

$$E_g(m_3 = 2 m_1) = \left[2 - \frac{1}{2 \zeta_1} \left\{ 1 + \left(\frac{v_{\rm in}}{v_{\rm esc,1}} \right)^2 \right\} \right] E_g(m_1). \tag{84}$$

And we can also estimate the radius r_3 after the collision event;

$$\frac{r_3}{r_1} = \frac{8 \zeta_3}{4 - \frac{1}{\zeta_1} \left\{ 1 + \left(\frac{v_{\rm in}}{v_{\rm esc,1}} \right)^2 \right\}}, \tag{85}$$

where $v_{\rm in}$ requires

$$v_{\rm in} \leq v_{\rm esc,1} \sqrt{4 \zeta_1 - 1}. \tag{86}$$